Circuits and Systems
Mekelweg 4,
2628 CD Delft
The Netherlands
http://ens.ewi.tudelft.nl/

CAS-2020-4793757

M.Sc. Thesis

Multi-target Detection and Tracking with 8 GHz FMCW Radar System

Siyan Wan M.Sc.

Abstract

Currently, most of FMCW radar systems for target detection and localization are based on the radar system with multiple receiving antennas, but little based on the SISO system. In this project, we will show a unique signal processing pipeline based on the 8 GHz SISO FMCW radar system. An advanced algorithm of multi-target detection and tracking will be designed to monitor the range, angle, and Doppler velocity information of targets.

Multi-target Detection and Tracking with 8 GHz FMCW Radar System

Thesis

submitted in partial fulfillment of the
requirements for the degree of

Master of Science

in

Electrical Engineering

by

Siyan Wan M.Sc.
born in Qujing, People's Republic of China

This work was performed in:

Circuits and Systems Group
Department of Microelectronics & Computer Engineering
Faculty of Electrical Engineering, Mathematics and Computer Science
Delft University of Technology

Delft University of Technology

Delft University of Technology
Department of
Microelectronics & Computer Engineering

The undersigned hereby certify that they have read and recommend to the Faculty of Electrical Engineering, Mathematics and Computer Science for acceptance a thesis entitled **"Multi-target Detection and Tracking with 8 GHz FMCW Radar System"** by **Siyan Wan M.Sc.** in partial fulfillment of the requirements for the degree of **Master of Science**.

Dated: 28, July, 2020

Chairman: _____
prof.dr.ir. A.J. van der Veen

Advisor: _____
dr. P. Nazemzadeh

Committee Members: _____
dr. F. Fioranelli

_____

Abstract

Currently, most of FMCW radar systems for target detection and localization are based on the radar system with multiple receiving antennas, but little based on the SISO system. In this project, we will show a unique signal processing pipeline based on the 8 GHz SISO FMCW radar system. An advanced algorithm of multi-target detection and tracking will be designed to monitor the range, angle, and Doppler velocity information of targets.

Acknowledgments

First of all, I would like to thank my supervisor, Prof. van der Veen, who gave me numerous valuable advice about my thesis project. He is always kind and patient to guide me step-by-step to finish this project. During the writing of this thesis. he has patiently reviewed this article and making suggestions to improve it.

Secondly, I want to thank my daily supervisor, Dr. Nazemzadeh for his assistance during this thesis project. He has provided me with great support and valuable guidance. He encouraged me to try some new ideas and helped me to solve the problems. I am very grateful for his encouragement and support.

Special thanks to the project group leader Dr. Peng and my colleague Lichen. They are very nice and patient. At the beginning of the thesis project, I was new in the radar field, and they helped me get familiar with the radar system. Because of their support and help, I could successfully adapt to new surroundings. They also gave me a lot of useful advice during the whole project.

Additionally, I need to express my massive gratitude to my family and my friends. They gave me the courage and strength to face challenges.

Siyan Wan M.Sc.
Delft, The Netherlands
28, July, 2020

Contents

Abstract **v**

Acknowledgments **vii**

1 Introduction **1**
1.1 Problem statement . . . 1
1.2 Related work . . . 1
1.3 Thesis objective . . . 2
1.4 Outline . . . 2

2 Data model **5**
2.1 Theoretical Background of FMCW radar . . . 5
2.2 Beam scanning . . . 8
2.3 Multipath propagation Model . . . 8
2.4 Multi-target Model . . . 10
2.5 Conclusion . . . 11

3 Pre-processing of the radar signal **13**
3.1 FMCW matrix . . . 13
3.2 Angular slide window . . . 15
3.3 Range-Doppler 2D FFT . . . 16
3.4 Conclusion . . . 19

4 Multi-target detection **21**
4.1 Background of CFAR algorithms . . . 21
4.2 Multi-target detection based on CFAR . . . 23
4.2.1 Problem statement . . . 23
4.2.2 3D OSGO CFAR . . . 23
4.2.3 Improved detection algorithm . . . 25
4.3 Clustering . . . 26
4.4 Conclusion . . . 27

5 Multi-target tracking **29**
5.1 Tracking model . . . 29
5.2 Linear Kalman prediction . . . 30
5.3 Data association . . . 31
5.3.1 GNN . . . 31
5.4 Linear Kalman update . . . 32
5.5 Conclusion . . . 33

6 Simulation and Evaluation **35**
6.1 Conclusion . . . 38

7 Experimental Validation **39**
7.1 Experimental platform 39
7.2 Experimental Results 40
7.3 Conclusion 46

8 Conclusion and future work **49**
8.1 Conclusion 49
8.2 Future work 49

List of Figures

2.1 The FMCW Radar system block 5
2.2 The signal of FMCW radar 6
2.3 Beam scanning for one chirp 8

3.1 Signal processing block of FMCW radar system 13
3.2 FMCW matrix 14
3.3 FMCW matrix with angle 15
3.4 2D FFT 17
3.5 Range-Doppler matrix with angle index $l = 3, \ldots, 17$ 18

4.1 Basic CFAR algorithm 22
4.2 OSGO CFAR processor 23
4.3 The distribution of reference cells 24
4.4 3D OSGO CFAR processor 25
4.5 3D OSGO CFAR with improved detection algorithm 26
4.6 Clustering for two targets 27

5.1 Multi-target tracking 29
5.2 Data association 32

6.1 The sketches of target trails for different scenarios 35
6.2 Range RMSE 36
6.3 Angle RMSE 37
6.4 Doppler velocity RMSE 38

7.1 FMCW radar platform 39
7.2 Experiment environment 40
7.3 Target tracks for different scenarios 41
7.4 The results of Scenario 1 43
7.5 The results of Scenario 2 44
7.6 The results of Scenario 3 45
7.7 The results of Scenario 4 46

List of Tables

7.1 Parameters of the 8 GHz FMCW radar system 40

1 Introduction

1.1 Problem statement

Nowadays, more and more applications (e.g. intelligent safeguard systems and smart lighting systems) have been designed for smart building. The sensor network monitors and provides real-time information of targets to other higher layer applications. Because of this, the accuracy of localization is important for the sensor network. Besides, real-time monitoring requires that sensor network is low-power and low-complexity. Compared to other image-based sensors, the frequency-modulated continuous-wave (FMCW) radar sensor has obvious advantages for privacy preservation and robustness of the light from the environment.

Currently, a lot of researches of indoor localization are based on the radar system with multiple receiving antennas. According to the phase difference and frequency difference, the position information and velocity information of targets can be easily obtained. However, there has been very little research intended to indoor localization with Single Input Single Output (SISO) FMCW radar system.

1.2 Related work

As a low-power, low-complexity sensor, FMCW radar system has been widely used in short-range detection for automotive application [18, 20, 25] and indoor localization [34, 35].

Currently, FMCW radar systems for target detection and localization are mostly based on Multiple Input Single Output(MISO) systems in K-band [12, 18, 20, 24, 39] and Multiple Input Multiple Output(MIMO) systems in W-band[19, 26, 30, 33]. The resolution and design complexity depend on the work frequency of the radar. The FMCW radar with higher frequency has a better resolution and beam-forming, but a higher complexity and power. However, only a few researches for the localization have considered the FMCW radar with lower frequency.

The signal processing pipelines for MISO and MIMO systems are similar. As the frequency difference between the transmitted signal and the echo signal carries range and Doppler velocity information of the target, 2D FFT and detection algorithms are used to detect the range and Doppler velocity of the target. The angle of arrival is estimated by the phase difference with the antenna array. Then, the paring algorithm is used to match the position and velocity information of the same target. Besides the typical Constant False-Alarm Rate (CFAR) detection [11, 36], the deep learning

method (e.g. Convolutional Neural network(CNN) [33]) can also be used for the target detection. As a typical SISO system cannot get angle information, few study of detecting target has focused on SISO FMCW radars.

For multi-target tracking algorithms, there are two main methods: 1) probabilistic hypothesis density (PHD) filter [9, 13, 14, 32], 2) Bayes filter with data association [8]. The PHD filter uses the random finite sets (RFS) of state and observation to replace the typical accurate state and measurement, which can remove the noise effectively. Compared to PHD filter, the data association method relies more on accuracy of the detection algorithm but has less computational complexity.

In summary, current multi-target detection algorithms mostly are based on the signal processing pipeline with MISO and MIMO radar systems instead of with the lower frequency SISO system. The main direction of current multi-target tracking algorithms is PHD filter. However, the performance of multi-target tracking with PHD filter comes at the expense of a high computational complexity, which is not suitable for real-time indoor target monitoring.

1.3 Thesis objective

The main objectives of this thesis project are:

. Design new signal processing pipeline for a SISO FMCW radar system

. Improve multi-target detection algorithm to increase the accuracy of detection.

. Optimize low-complexity multi-target tracking algorithm for cases where targets appear and disappear.

In this project, we consider a methodology for multi-target detection and tracking for an 8 GHz SISO FMCW radar system. To locate multiple targets with a SISO radar system, a new signal processing pipeline different from MIMO or MISO signal processing has to be designed. Time domain sliding window will be adopted to estimate the angle information of targets. For detection and tracking, an improved multi-target detection algorithm will be adopted to reduce the background noise and improve the detection accuracy. Multi-target tracking algorithms with data association also offer some improvements for cases where targets appear and disappear.

1.4 Outline

The structure of this report is as follows:

. Chapter 2 will introduce the basic data model of an FMCW radar and extend the basic data model of a radar signal to the multipath propagation and multi-target cases.

. Chapter 3 will introduce the pre-processing of FMCW radar signals which can transfer the time domain radar signal to a joint range, Doppler, and angle domain signal.

. An improved multi-target detection algorithm will be presented in Chapter 4.

. Chapter 5 will derive the multi-target tracking algorithm.

. Chapter 6 will introduce the simulation model and evaluate the simulation results.

. Chapter 7 will show the results of experimental data with real FMCW radar system.

. The last chapter lists the conclusions and future work.

Data model

2

In a general SISO FMCW radar system, a low-frequency FMCW waveform is mixed with a local oscillator signal and generates the modulated signal, which will be sent by a transmitting antenna. The receiving antenna receives the echo signal reflected by the objects. From the frequency difference between the transmitted signal and the received signal, we can obtain the range and Doppler velocity of targets.

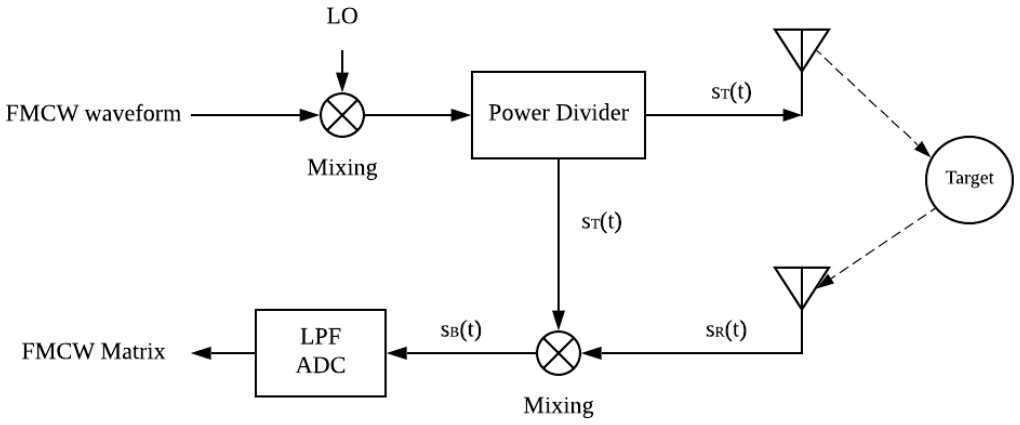

Figure 2.1: The FMCW Radar system block

2.1 Theoretical Background of FMCW radar

In this project, a intra-pulse chirp beam scanning signal (shown in Figure 2.2) is used as FMCW signal. The frequency of the transmitted signal is modulated linearly such that the starting frequency f_c is 7.3 GHz and the bandwidth B is 1 GHz.

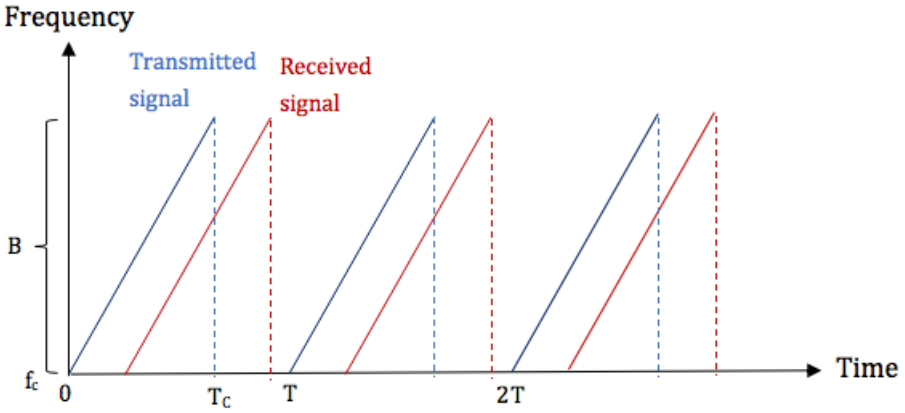

Figure 2.2: The signal of FMCW radar

Assume that time t can be divided into

$$t = nT + t_s,\ 0 < t_s < T \tag{2.1}$$

where T_c is the sweep time and T is interval between two chirps.

The instantaneous frequency of the transmitted signal increases linearly for one chirp. This can be expressed as

$$f(t) = f_c + \rho t_s,\ 0 \leq t_s \leq T_c \tag{2.2}$$

where f_c is the starting frequency and B is the bandwidth. $\rho = \frac{B}{T_c}$ is the rate of the frequency increase.

As the transmitted signal is not continuous, the instantaneous phase of the transmitted signal is only related to the current chirp:

$$\begin{aligned} \phi(nT + t_s) &= 2\pi \int_0^{t_s} f(t)dt + \varphi_0 \\ &= 2\pi(f_c t_s + \frac{\rho}{2} t_s^2) + \varphi_0 \end{aligned} \tag{2.3}$$

where φ_0 is the initial phase.

Therefore, the complex form of the transmitted signal is

$$s_T(t) = a_T e^{j\phi(t)} = a_T e^{j(2\pi(f_c t_s + \frac{\rho}{2} t_s^2) + \varphi_0)} \tag{2.4}$$

where a_T is the amplitude of the transmitted signal.

The transmitted signal is reflected by the object and then received by the receiving antenna. The received signal $s_R(t)$ can be regarded as a signal attenuated and delayed version of the transmitted signal,

$$s_R(t) \propto s_T(t - \tau(t)) \tag{2.5}$$

With an object in linear motion, the time delay $\tau(t)$ denotes the round-trip time between the radar and the object.

$$\tau(t) = \frac{2(R+vt)}{c} = \frac{2(R+v(nT+t_s))}{c} \tag{2.6}$$

where R is the initial distance of object, v is the Doppler velocity, and c is the speed of light.
The received signal can be expressed as

$$s_R(t) = a_R e^{j\phi(t-\tau(t))} = a_R e^{j(2\pi(f_c(t_s-\tau(t))+\frac{\rho}{2}(t_s-\tau(t))^2)+\varphi_0)} \tag{2.7}$$

where a_R is the amplitude of received signal.

By mixing the transmitted signal and received signal, we can get the beat-frequency signal:

$$\begin{aligned} s_B(t) &= a_T e^{j\phi(t)} a_R e^{-j\phi(t-\tau(t))} \\ &= a_T a_R e^{j(2\pi(f_c t_s+\frac{\rho}{2}t_s^2)+\varphi_0)} e^{-j(2\pi(f_c(t_s-\tau(t))+\frac{\rho}{2}(t_s-\tau(t))^2)+\varphi_0)} \\ &= a_T a_R e^{j2\pi(f_c\tau(t)+\rho\tau(t)t_s-\frac{\rho}{2}\tau(t)^2)} \end{aligned} \tag{2.8}$$

According to Equation (2.6),

$$\begin{aligned} s_B(t) &= a_T a_R e^{j2\pi(f_c\frac{2(R+v(nT+t_s))}{c}+\rho t_s\frac{2(R+v(nT+t_s))}{c}-\frac{2\rho(R+v(nT+t_s))^2}{c^2})} \\ &= a_T a_R e^{j2\pi[(\frac{2f_cR}{c}-\frac{2\rho R^2}{c^2})+t_s(\frac{2f_cv}{c}+\frac{2\rho R}{c}+\frac{2\rho vnT}{c}-\frac{4\rho v^2nT}{c^2}-\frac{4\rho Rv}{c^2})+t_s^2(\frac{2\rho v}{c}-\frac{2\rho v^2}{c^2})+nT(\frac{2f_cv}{c}-\frac{4\rho Rv}{c^2})-\frac{2\rho v^2n^2T^2}{c^2}]} \end{aligned} \tag{2.9}$$

As c is the speed of light and $v \ll c$, the terms with c^2 in the denominator are quite small and can be neglected [31]. The beat-frequency signal can be simplified and rewritten as

$$\begin{aligned} s_B(t) &\approx a_T a_R e^{j2\pi[\frac{2f_cR}{c}+(\frac{2f_cv}{c}+\frac{2\rho R}{c}+\frac{2\rho vnT}{c})t_s+\frac{2\rho v}{c}t_s^2+nT\frac{2f_cv}{c}]} \\ &\approx a_T a_R e^{j2\pi\frac{2f_cR}{c}} e^{j2\pi\frac{2f_cv}{c}nT} e^{j2\pi\frac{2\rho R}{c}t_s} \\ &= a_B e^{j2\pi f_d nT} e^{j2\pi f_b t_s} \end{aligned} \tag{2.10}$$

with $t = nT + t_s$.
The amplitude of the beat-frequency signal a_B, Doppler frequency f_d, and beat frequency f_b are:

$$a_B = a_T a_R e^{j2\pi\frac{2f_cR}{c}} \tag{2.11}$$

$$f_d = \frac{2f_cv}{c} \tag{2.12}$$

$$f_b = \frac{2\rho R}{c} \tag{2.13}$$

2.2 Beam scanning

Our FMCW radar system is a SISO radar system with one transmitting antenna and one receiving antenna. Both antennas are specially designed frequency scanning antennas with "rampart" shape. In this 8 GHz FMCW radar, the main direction of the antenna beam changes linearly with increasing signal frequency. As the instantaneous frequency of transmitted signal increases linearly for one chirp, there is a linear relationship between the main direction of the antenna beam and fast time t_s. For one chirp, the antenna scans different angle in different time.

The main direction angle of the beam is

$$\theta(t) = \theta_0 + \mu(f(t) - f_c) = \theta_0 + \alpha t_s \tag{2.14}$$

where θ_0 is the initial angle and α is the rate of angle increase.

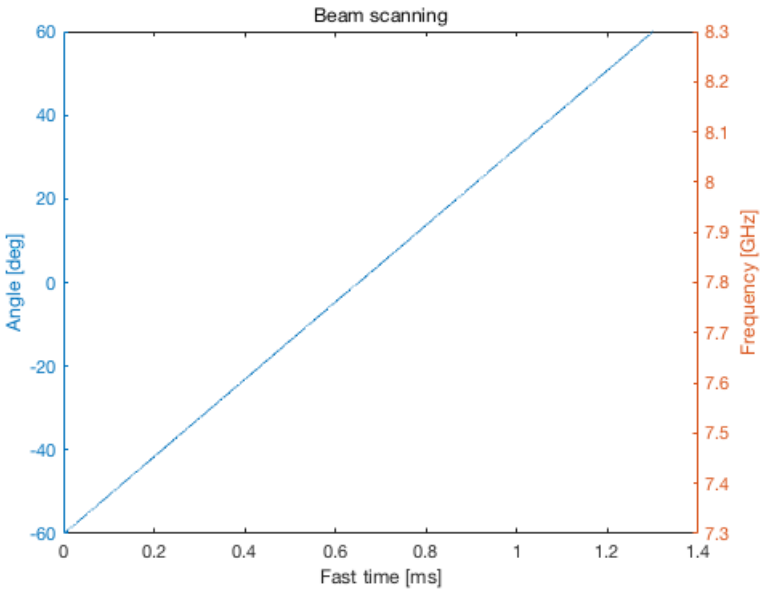

Figure 2.3: Beam scanning for one chirp

Based on this feature, for each chirp, the main direction of beam can sweep from -2 deg to 60 deg with 1 GHz scanning bandwidth. If we change the direction of excitement, the radar will sweep the other symmetrical sector with 2 deg to -60 deg. In this project, the radar scans both sectors from -60 deg to 60 deg, which can be seen in Figure 2.3.

2.3 Multipath propagation Model

As our FMCW radar system is designed for an indoor environment, the received signal will not only come from one reflected path. It is necessary to consider the effect of multipath interference.

For the basic propagation model, the signal propagation between the transmit antenna and the receive antenna can also be expressed by an impulse response function $h(t)$ [29]. According to Equation (2.4), the received signal $s_R(t)$ can be rewritten as

$$s_R(t) = h(t) * s_T(t) = \beta\delta(t - \tau(t)) * s_T(t) \tag{2.15}$$

$$h(t) = \beta\delta(t - \tau(t)) \tag{2.16}$$

where β is the gain of path, $\delta(.)$ is Dirac delta function, and $\tau(t)$ is the time delay.

Next, we extend the impulse response function to a multipath propagation model. Assume that the received signal of one object has L reflected paths. The multi-channel impulse response function $h(t)$ can be rewritten as

$$h(t) = \sum_{j=1}^{L} h_j(t) = \sum_{j=1}^{L} \beta_j\delta(t - \tau_j(t)) \tag{2.17}$$

where $h_j(t)$ is the impulse response function of path j, β_j is the gain of path j, and $\tau_j(t)$ is the delay of path j.

Therefore, the received signal for a multipath propagation model becomes

$$\begin{aligned} s_R(t) &= \left[\sum_{j=1}^{L} \beta_j\delta(t - \tau_j(t))\right] * s_T(t) \\ &= \sum_{j=1}^{L} \beta_j s_T(t - \tau_j(t)) \\ &= \sum_{j=1}^{L} a_{R_j} e^{j(2\pi(f_c(t_s - \tau_j(t)) + \frac{\rho}{2}(t_s - \tau_j(t))^2) + \varphi_0)} \end{aligned} \tag{2.18}$$

where a_{R_j} is the amplitude of received signal of path j.

Then, the beat-frequency signal $s_B(t)$ can be rewritten as

$$\begin{aligned} s_B(t) &= s_T(t) \cdot s_R^*(t) \\ &= \sum_{j=1}^{L} a_T a_{R_j} e^{j2\pi(f_c\tau_j(t) + \rho\tau_j(t)t_s - \frac{\rho}{2}\tau_j(t)^2)} \\ &= \sum_{j=1}^{L} s_{B_j}(t) \end{aligned} \tag{2.19}$$

where $s_{B_j}(t)$ denotes the beat-frequency signal of path j, and is given by

$$s_{B_j}(t) = a_T a_{R_j} e^{j2\pi(f_c\tau_j(t) + \rho\tau_j(t)t_s - \frac{\rho}{2}\tau_j(t)^2)} \tag{2.20}$$

2.4 Multi-target Model

As the objective of this project is to detect and track multiple targets with an FMCW radar, the data model should also consider the multi-target case. Assume that the number of targets is N. The received signal of target i has L_i reflected paths.

Assume that the environment background noise $n(t)$ is homogeneous. Considering the reflection of multiple targets and background noise, the received signal can be rewritten as

$$s_R(t) = \sum_{i=1}^{N} \sum_{j=1}^{L_i} h_{ij}(t) * s_T(t) + n(t) \tag{2.21}$$

$$h_{ij}(t) = \beta_{ij}\delta(t - \tau_{ij}) \tag{2.22}$$

where i is the target index, β_{ij} is the gain of target i with path j, and τ_{ij} is the delay of target i with path j.

Then, the beat-frequency signal with noise can be expressed as

$$\begin{aligned} s_B(t) &= \sum_{i=1}^{N} \sum_{j=1}^{L_i} a_T a_{R_{ij}} e^{j2\pi(f_c\tau_{ij} + \rho\tau_{ij}t_s - \frac{\rho}{2}\tau_{ij}^2)} + n(t)s_T(t) \\ &\approx \sum_{j=1}^{N} \sum_{j=1}^{L_i} s_{B_{ij}}(t) + n_B(t) \end{aligned} \tag{2.23}$$

where $a_{R_{ij}}$ is the amplitude of received signal of target i with path j, and $n_B(t)$ is the noise of the beat-frequency signal after low pass filtering.
The beat frequency signal of target i with path j is given by

$$s_{B_{ij}}(t) = a_T a_{R_{ij}} e^{j2\pi(f_c\tau_{ij} + \rho\tau_{ij}t_s - \frac{\rho}{2}\tau_{ij}^2)} \tag{2.24}$$

where τ_{ij} is the delay of target i with path j.

Assume the Doppler velocity of target i with path j is v_{ij} and the range of target i with path j is R_{ij}. Then, the delay can be express as

$$\tau_{ij}(t) = \frac{2(R_{ij} + v_{ij}t)}{c} \tag{2.25}$$

Similar with Equation (2.10), the beat frequency signal of target i with path j:

$$s_{B_{ij}}(t) = a_{B_{ij}} e^{j2\pi f_{d_{ij}} nT} e^{j2\pi f_{b_{ij}} t_s} \tag{2.26}$$

with $t = nT + t_s$.

$$f_{d_{ij}} = \frac{2f_c v_{ij}}{c} \tag{2.27}$$

$$f_{b_{ij}} = \frac{2\rho R_{ij}}{c} \tag{2.28}$$

where $f_{d_{ij}}$ is the Doppler frequency, and $f_{b_{ij}}$ is the beat frequency.

Assume the angle of target i with path j is θ_{ij}. Considering beam scanning of antenna, the radar can receive signal from target i with path j only in a certain time with $t_s = t_{s_{ij}}$. According to Equation (2.14), $t_{s_{ij}}$ can be expressed as

$$t_{s_{ij}} = \frac{1}{\alpha}(\theta_{ij} - \theta_0) \tag{2.29}$$

Then, the beat frequency signal of target i with path j can be rewritten as

$$\begin{aligned} s_{B_{ij}}(t) &= a_{B_{ij}} e^{j2\pi f_{d_{ij}} nT} e^{j2\pi f_{b_{ij}} t_s} \delta(t_s - t_{s_{ij}}) \\ &= a_{B_{ij}} e^{j2\pi f_{d_{ij}} nT} e^{j2\pi f_{b_{ij}} t_s} \delta(t_s - \frac{1}{\alpha}(\theta_{ij} - \theta_0)) \end{aligned} \tag{2.30}$$

2.5 Conclusion

In this chapter, we have introduced the background theories of SISO FMCW radar system and established the data model of signal processing with multipath propagation and multi-target cases. The data model will be the basis of the whole signal processing pipeline.

Pre-processing of the radar signal

3

The signal processing of the FMCW radar system can be divided into three parts: pre-processing, multi-target detection, and multi-target tracking, which can be seen in Figure 3.1. To locate the target in real-time, we set N_d chirps as a frame. we pre-process and detect targets from the radar signal of each frame, and apply the detection results of different frames to multi-target tracking.

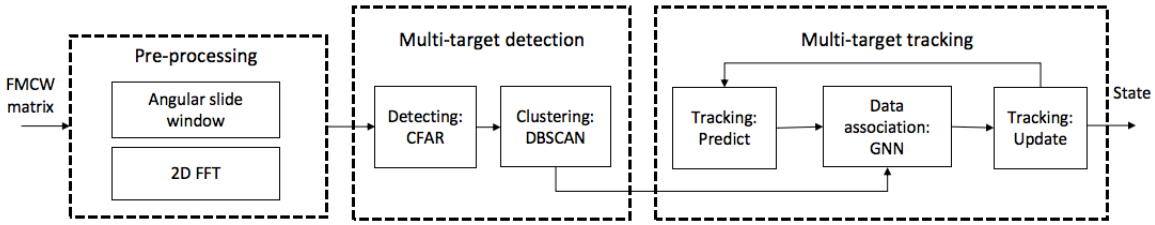

Figure 3.1: Signal processing block of FMCW radar system

This chapter will mainly discuss the pre-processing of the FMCW radar signal. The details of multi-target detection and tracking will be introduced in next Chapters.

In this chapter, we will introduce the initial point of signal processing, FMCW matrix, and the two steps of pre-processing. With angular slide window and 2D FFT, the time domain FMCW matrix can be transform into Doppler velocity, range and angle domain and generate the 3D feature matrix.

3.1 FMCW matrix

For the first frame, after low-pass filtering and ADC sampling, the beat frequency signal $s_B(t)$ (Equation (2.23)) is discretized by in-chirp sampling, and chirp-by-chirp sampling. Let $t = nT + t_s$, and sample t_s as $t_s = m/f_s$ with the sample rate f_s. nT is called slow time, while $t_s = m/f_s$ is fast time. Then, the number of bins for one chirp is $M = f_s T_c$.

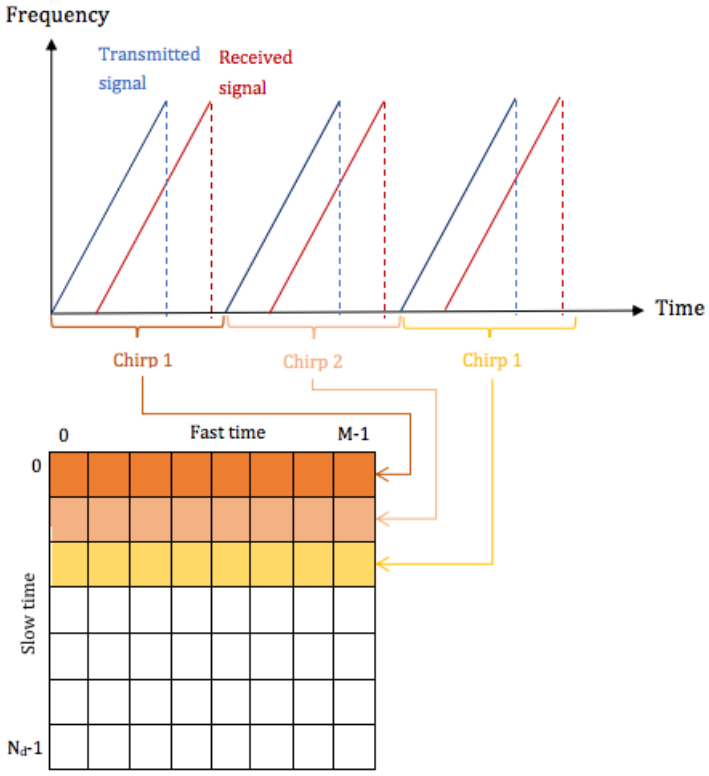

Figure 3.2: FMCW matrix

The $N_d \times M$ matrix generated by the discretized beat-frequency signal is defined as the FMCW matrix

$$\mathbf{S_B} = \begin{bmatrix} s_B(0,0) & s_B(0,1) & \cdots & s_B(0,M-1) \\ s_B(1,0) & s_B(1,1) & \cdots & s_B(1,M-1) \\ \vdots & \vdots & & \vdots \\ s_B(N_d-1,0) & s_B(N_d-1,1) & \cdots & s_B(N_d-1,M-1) \end{bmatrix} \tag{3.1}$$

$$s_B(n,m) = \sum_{i=1}^{N} \sum_{j=1}^{L_i} s_{B_{ij}}(n,m) + n_B(n,m) \tag{3.2}$$

$$0 \leq n \leq N_d - 1,\ 0 \leq m \leq M-1$$

where $n_B(n,m)$ is the noise of the discretized beat-frequency signal.

Based on Equation (2.30), the discredized beat frequency of target i with path j can be expressed as

$$s_{B_{ij}}(n,m) = a_{B_{ij}} e^{j2\pi f_{d_{ij}} nT} e^{j2\pi f_{b_{ij}} \frac{m}{f_s}} \delta(\frac{m}{f_s} - \frac{1}{\alpha}(\theta_{ij} - \theta_0)) \tag{3.3}$$

$$1 \leq i \leq N,\ 1 \leq j \leq L_i$$

where N is the number of targets and L_i is the number of reflected paths for target i.

3.2 Angular slide window

For MIMO and MISO systems, the angle of arrival estimation is based on the phase difference from the antenna array. However, as a SISO system only has single receiving antenna, we cannot use the same method to estimate the angle information. In this project, a new method is needed to extract the angle information for the SISO FMCW radar system.

As the chirp frequency shows a linear change with time for one chirp, the original received signal can be divided into different angle signals using sliding window in time domain. Several sliding windows belonging to different angles are used in each row of the FMCW matrix. Each sliding window should be designed to enhance the signal of one specific angle and reduce the signal belonging other angles.

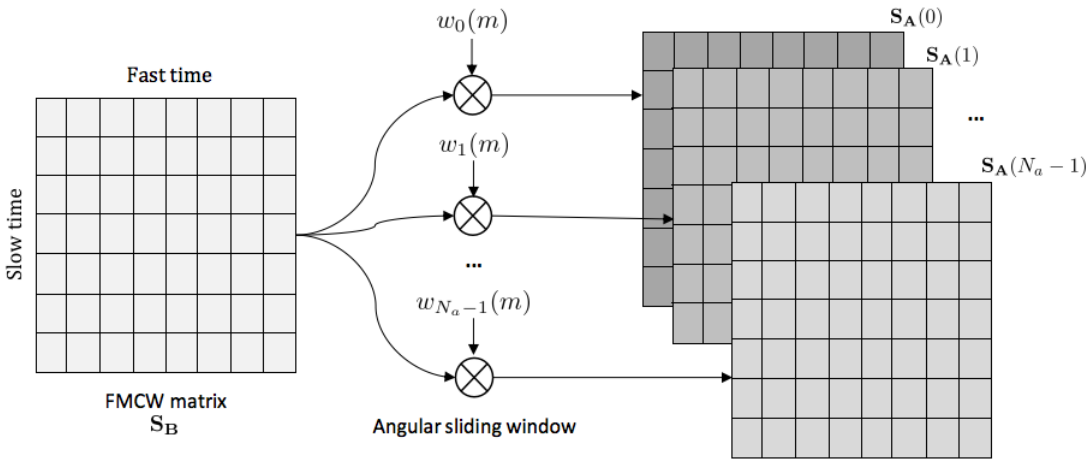

Figure 3.3: FMCW matrix with angle

Assume that the number of the sliding windows is N_a. The step size of the angel depends on the number of sliding windows. According to Equation (2.14), the angle resolution is denoted by $\Delta\theta = \frac{\alpha T_c}{N_a}$.

After performing the angular sliding window in fast time domain, we can get a new $N_d \times M \times N_a$ time domain array:

$$\mathbf{S_A} = s_A(n, m, l) = s_B(n, m) w_l(m) \tag{3.4}$$

$$0 \leq l \leq N_a - 1$$

$w_l(.)$ is the angular sliding window for angle $\theta_l = \theta_0 + \Delta\theta l$ in time domain. Consider avoid spectrum leakage, we use Hamming window to generate the angular sliding window [27].

$$w_l(m) = w(m)\delta(m - \frac{f_s}{\alpha}(\theta_l - \theta_0) + \frac{N_w}{2}) = w(m)\delta(m - \frac{f_s}{\alpha}\Delta\theta l + \frac{N_w}{2}) \tag{3.5}$$

where $w(.)$ is the Hamming window

$$w(n) = \begin{cases} 0.54 - 0.46\ cos(\dfrac{2\pi n}{N_w - 1}) & 0 \leq n \leq N_w - 1 \\ 0 & other \end{cases} \tag{3.6}$$

N_w is the width of Hamming window in samples.

Then, the FMCW matrix of angle θ_l can be rewritten as

$$\begin{aligned} s_A(n, m, l) &= \left[\sum_{i=1}^{N}\sum_{j=1}^{L_i} s_{B_{ij}}(n, m) + n_B(n, m)\right] w_l(m) \\ &= \sum_{i=1}^{N}\sum_{j=1}^{L_i} s_{A_{ij}}(n, m, l) + n_A(n, m, l) \end{aligned} \tag{3.7}$$

$$\begin{aligned} s_{A_{ij}}(n, m, l) &= s_{B_{ij}}(n, m)w_l(m) \\ &\approx a_{B_{ij}} e^{j2\pi f_{d_{ij}} nT} e^{j2\pi f_{b_{ij}} \frac{m}{f_s}} \delta(\theta_{ij} - (\theta_0 + \Delta\theta l)) \end{aligned} \tag{3.8}$$

where $n_A(n, m, l)$ is the noise of the beat frequency signal after angular sliding window.

3.3 Range-Doppler 2D FFT

The time domain matrix with angle index l is defined as

$$\mathbf{S_A}(l) = [s_A(n, m, l)|\ 0 \leq n \leq N_d,\ 0 \leq n \leq M] \tag{3.9}$$

To get the range and velocity information of targets, the Fast Fourier Transform algorithm is used to process the matrices $\mathbf{S_A}(l),\ l = 0,\ 1,\ \ldots N_a - 1$.

First, perform an FFT to the fast-time domain of the matrix $\mathbf{S_A}(l)$. Different rows correspond to chirps at different time. Then, perform an FFT to the slow-time domain to generate range-Doppler matrix [37].

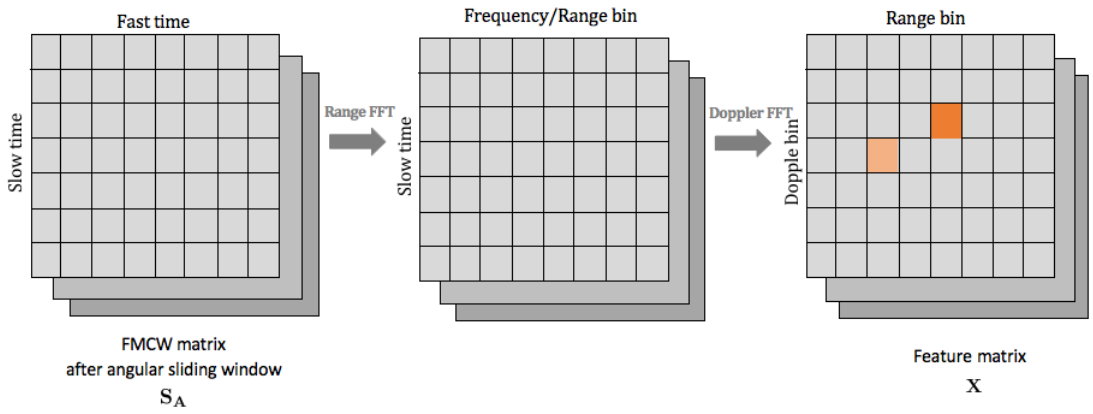

Figure 3.4: 2D FFT

Ignoring the side lobe effect of window function, the 3D feature array can be expressed as

$$\begin{aligned}\mathbf{X} = x(p,q,l) &= \sum_{n=0}^{N_d-1}\left[\sum_{m=0}^{M-1} s_A(n,m,l)e^{-j\frac{2\pi}{M}qm}\right]e^{-j\frac{2\pi}{N_d}pn} \\ &= \sum_{i=1}^{N}\sum_{j=1}^{L_i} s_{ij}(p,q,l) + n_x(p,q,l)\end{aligned} \tag{3.10}$$

$$\begin{aligned}s_{ij}(p,q,l) &= \sum_{n=0}^{N_d-1}\left[\sum_{m=0}^{M-1} s_{A_{ij}}(n,m,l)e^{-j\frac{2\pi}{M}qm}\right]e^{-j\frac{2\pi}{N_d}pn} \\ &= A_{ij}\delta(\frac{q}{M} - \frac{f_{b_{ij}}}{f_s})\delta(\frac{p}{N_d} - f_{d_{ij}}T)\delta(\theta_{ij} - (\theta_0 + \Delta\theta l))\end{aligned} \tag{3.11}$$

where $n_x(p,q,l)$ is the noise after 2D FFT, and $s_{ij}(p,q,l)$ is the frequency domain signal of the taget i with path j. p, q are the new index of Doppler bins and range bins.

As $s_{ij}(p,q,l)$ carries the beat frequency, Doppler frequency and angle information of target i with path j, we can easily estimate R_{ij} v_{ij} and θ_{ij} by detecting $s_{ij}(p,q,l)$ from feature array $\mathbf{X}$.

In this project, set the number of the sliding windows $N_a = 20$. To show the result of pre-processing, We simulate two moving targets, target 1 and target 2. At one frame, the range, Doppler velocity, and angle of target 1 are 4.03 m, -0.78 m/s, and -18.64 deg, while the range, Doppler velocity, and angle of target 2 are 4.32 m, 0.90 m/s, and 17.51 deg.

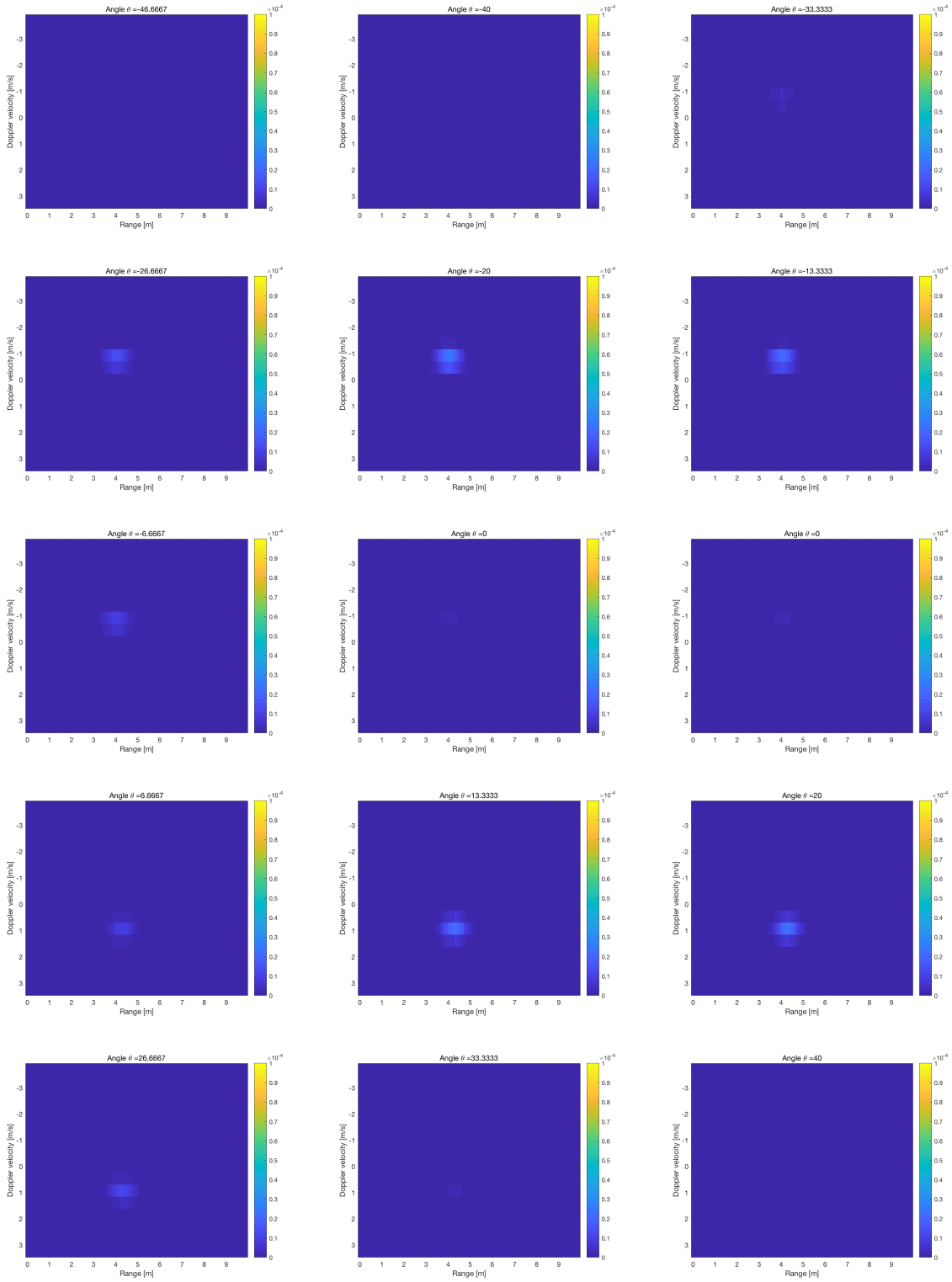

Figure 3.5: Range-Doppler matrix with angle index $l = 3, \ldots, 17$

The feature array after pre-processing can be seen in Figure 3.5. We will show

the Rang-Doppler plot with angle index $l = 3, \ldots, 17$. The indexes of feature array p, q, l have corresponding Doppler velocity, range, and angle value. To show the results clearly, we use the Doppler velocity, range, and angle value to replace the indexes of feature array in the figures.

From Figure 3.5, we can clearly see that Rang-Doppler plot with angle -13.33 deg and -20 deg has the signal of one target, and Rang-Doppler plot with angle 13.33 deg and 20 deg has the signal of the other signal. The pre-processing results correspond to true values of simulated targets.

3.4 Conclusion

In this chapter, we have introduced a unique pre-processing method for SISO FMCW radar system. The pre-processing method uses time-domain angular sliding windows to extract angle information of targets and uses 2D FFT to obtain range, Doppler velocity information. After pre-processing, we can obtain a 3D feature array from the time domain radar signal.

4 Multi-target detection

After pre-processing the FMCW radar signal and generating a feature array, we need a detection algorithm to determine whether targets exist in the feature array with background noise and clutter. In this project, considering the cases of target appearing and disappearing, the number of targets is unknown and inconstant. The main idea of the multi-target detection algorithm is based on Constant False-Alarm Rate(CFAR) method. To remove the effects of noise and multipath propagation, the clustering algorithm is also needed after the CFAR detection.

4.1 Background of CFAR algorithms

Before deriving multi-target detection algorithm, we will briefly introduce the basic CFAR algorithms for one dimensional signal sequence.

Consider a noisy signal sequence $x(i),\ i = 1,\ 2,\ \ldots, L$. The detection model of $x(i)$ can be expressed as

$$\begin{cases} H_0 : x(i) = n(i) \\ H_1 : x(i) = s(i) + n(i) \end{cases} \tag{4.1}$$

If the noise power σ_n^2 is known and constant, then we can define the threshold $T = f\sigma_n^2$ with factor f and define H_0 if $y(i) = x(i)^2 < T$. This leads to a constant false alarm rate P_{fa}. However, in most cases, the noise power σ_n^2 is inconstant. If we want to keep a constant P_{fa}, the factor f has to vary with the different noise power. We can estimate the local noise power and use the certain relationship between f, σ_n^2, and P_{fa} to generate factor f and threshold T. This is the main idea of CFAR method. The basic block of CFAR can be seen in Figure 4.2.

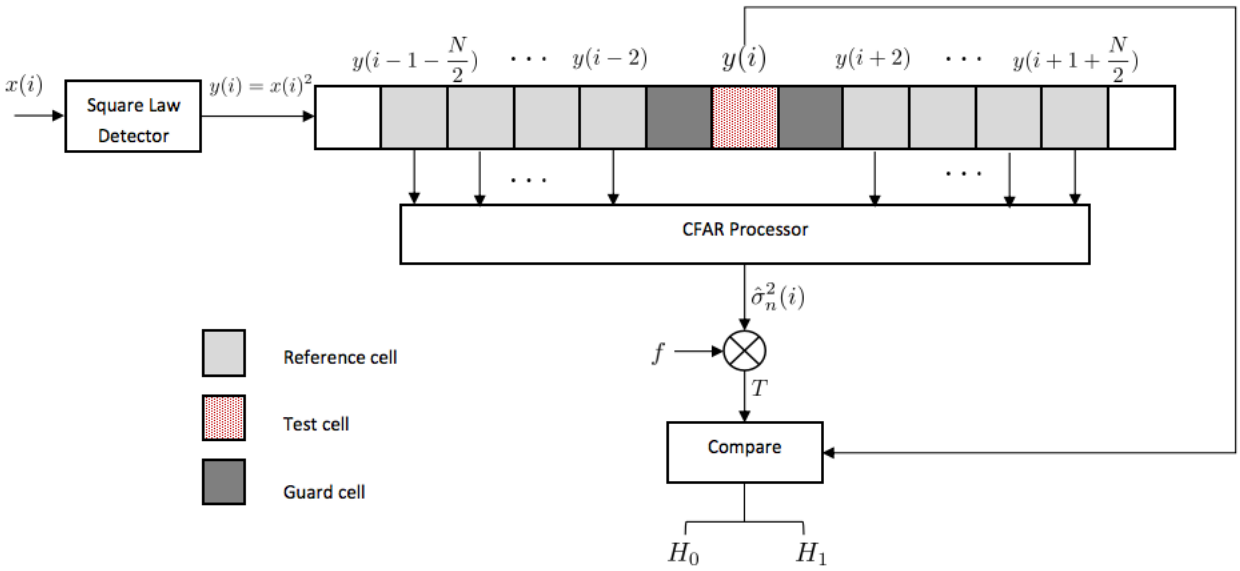

Figure 4.1: Basic CFAR algorithm

Assume that $x(i)$ is the test cell. We define the N neighbors of $x(n)$ as the reference cells and define the closest right and left neighbours as guard cells. Then, use the reference cells to estimate the local noise power of $x(i)$. Different CFAR methods adopt different strategies of estimation (CFAR processor) [7].

For the Ordered statistics Greatest of (OSGO) CFAR, the CFAR processor has three steps:

. Sort the right neighbor reference cells and left neighbor reference cells independently.

. Select the k_{th} smallest reference cells of both sides, which are denoted by $y_1(i)$ and $y_2(i)$.

. Select the maximum of $y_1(i)$ and $y_2(i)$ as the estimate of local noise power $\hat{\sigma}_n^2(i)$, i.e. $\hat{\sigma}_n^2(i) = max(y_1(i), y_2(i))$

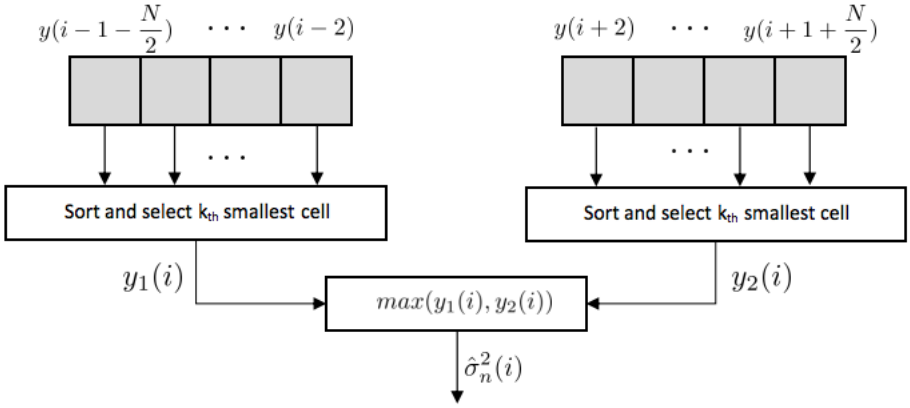

Figure 4.2: OSGO CFAR processor

According to the certain relationship between false alarm rate P_{fa} and factor f [3], if we set a constant P_{fa}, we can get the factor f and generate the threshold for $x(i)$.

4.2 Multi-target detection based on CFAR

4.2.1 Problem statement

Simply speaking, the multi-target detection is to find the local maximum in the feature array $\mathbf{X}$. Similar with Equation (4.1), we define the model for the multi-target detection:

$$\begin{cases} H_0: \ x(p,q,l) = n_x(p,q,l) \\ H_1: \ x(p,q,l) = \sum_{i=1}^{N} \sum_{j=1}^{L_i} s_{ij}(p,q,l) + n_x(p,q,l) \end{cases} \tag{4.2}$$

According to the index p, q, l of the cell with H_1, we can get the corresponding range, Doppler velocity, and angle information. As the corresponding index of feature array for different target and path are different, assume that each cell with H_1 only includes one target with strongest target signal in p, q, l.

Then, the detection model can be simplified and rewritten as

$$\begin{cases} H_0: \ x(p,q,l) = n_x(p,q,l) \\ H_1: \ x(p,q,l) = \max\limits_{0 \le i \le N, 0 \le j \le L_i} s_{ij}(p,q,l)) + n_x(p,q,l) \end{cases} \tag{4.3}$$

The corresponding range, Doppler velocity, and angle of $x(p,q,l)$ with H_1 belong to target i which maximize $s_{ij}(p,q,l)$.

4.2.2 3D OSGO CFAR

The typical method to detect targets is use 2D CFAR in Range-Doppler domain [15, 28] and angle of arrival estimation in angle domain [10]. Then, use a paring

algorithm to match the range, Doppler velocity and angle of the same target. This detection method needs the paring algorithm with high accuracy. In this project, we use multi-target detection based on 3D OSGO-CFAR, which is not need to use paring algorithm.

To detect targets in 3D feature array, we extend the 1D OSGO CFAR into three dimensions. Assume that the test cell is $x(p, q, l)$. The distribution of reference cells can be seen in Figure 4.5.

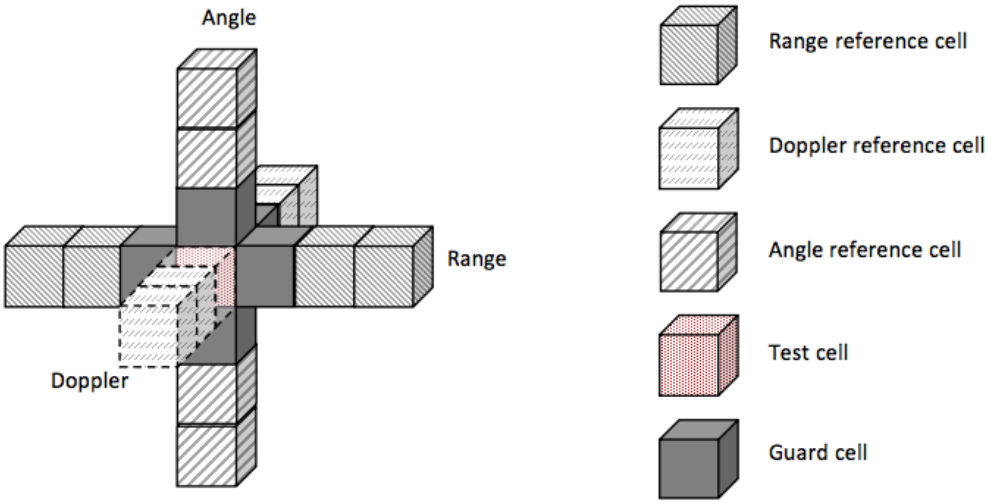

Figure 4.3: The distribution of reference cells

Then, the CFAR processor for three dimensional detection will become:

. Sort the Doppler reference cells, range reference cells, and angle reference cells independently.

. Select the k_{th} smallest reference cells for Doppler, range, and angle reference cells, which are denoted by $y_1(p, q, l)$, $y_2(p, q, l)$ and $y_3(p, q, l)$.

. Select the maximum of $y_1(p, q, l)$, $y_2(p, q, l)$ and $y_3(p, q, l)$ as the estimate of local noise power $\hat{\sigma}_n^2(p, q, l)$, i.e. $\hat{\sigma}_n^2(p, q, l) = max(y_1(p, q, l), y_2(p, q, l), y_3(p, q, l))$

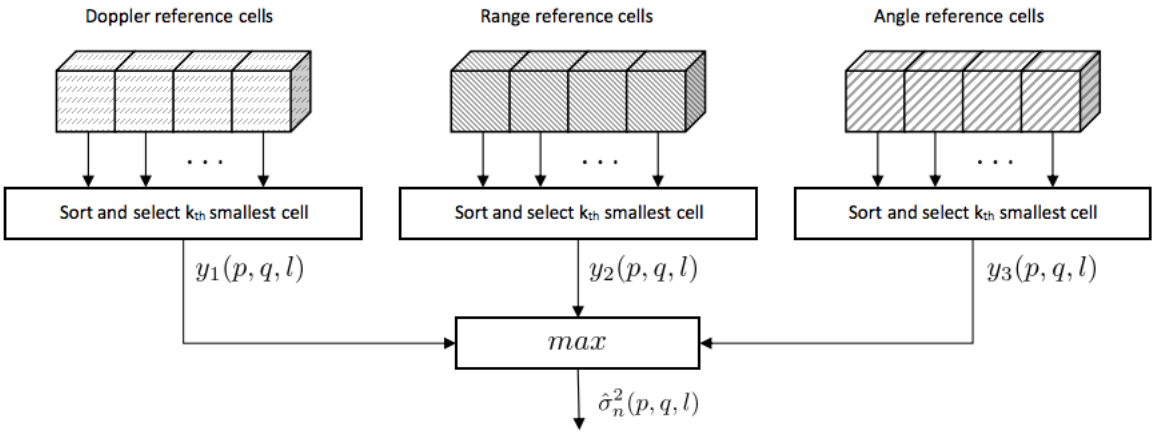

Figure 4.4: 3D OSGO CFAR processor

Similar with 1D OSGO CFAR, the factor f can be computed by the given constant false alarm P_{fa} [3]. Then we can get a threshold T to decide which hypothesis $x(p,q,l)$ belongs to.

If $x(p,q,l)$ belongs to H_1, there is a target signal in $x(p,q,l)$. The range, Doppler velocity and angle of the target can be given by index of $x(p,q,l)$. According to Equation (3.11), Equation (2.28), and Equation (2.27), the corresponding range, Doppler velocity and angle of the index p,q,l can be expressed as

$$R(q) = \frac{f_s c}{2\rho M} q = \Delta R q \tag{4.4}$$

$$v(p) = \frac{c}{2N_d T f_c} p = \Delta v p \tag{4.5}$$

$$\theta(l) = \theta_0 + \Delta\theta l \tag{4.6}$$

where $\Delta R,\ \Delta v,\ \Delta\theta$ are the range, Doppler velocity and angle resolution.

The measurement vector of $x(p,q,l)$ with H_0 is denoted as

$$\hat{\mathbf{z}}_u = [R(q), v(p), \theta(l)]^T \tag{4.7}$$

We perform 3D CFAR for each cell in feature array $\mathbf{X}$. Assume that the total number of detection results of feature array is U.

4.2.3 Improved detection algorithm

Assume that $x(p_0,q_0,l_0)$ has been already detected and the detection result is H_1. If $x(p_0,q_0,l_0)$ is used as reference cell for other test cell, $x(p_0,q_0,l_0)$ with H_1 will lead to

a large increase of the estimate of local noise power and threshold. This is also defined as masking effect [15]. As the masking effect cause more miss detection, a improved algorithm is necessary for multi-target detection.

The idea of the improved detection algorithm comes from CLEAN algorithm [17], but simplify the CLEAN algorithm. The main idea of this algorithm is "removing" detected target signal from the reference cells to reduce the masking effects [38]. When we have detected $x(p_0, q_0, l_0)$ with H_1, we add a feedback and reset the value of test cell as $\sigma_n(p_0, q_0, l_0)$. Then, if the test cell is $x(p_1, q_1, l_1)$, while $x(p_0, q_0, l_0)$ is the reference cell of $x(p_1, q_1, l_1)$, $\sigma_n(p_0, q_0, l_0)$ will be replace the true value of $x(p_0, q_0, l_0)$ to estimate $\sigma_n^2(p_1, q_1, l_1)$. The feedback can reduce the masking effects caused by detected local maximum.

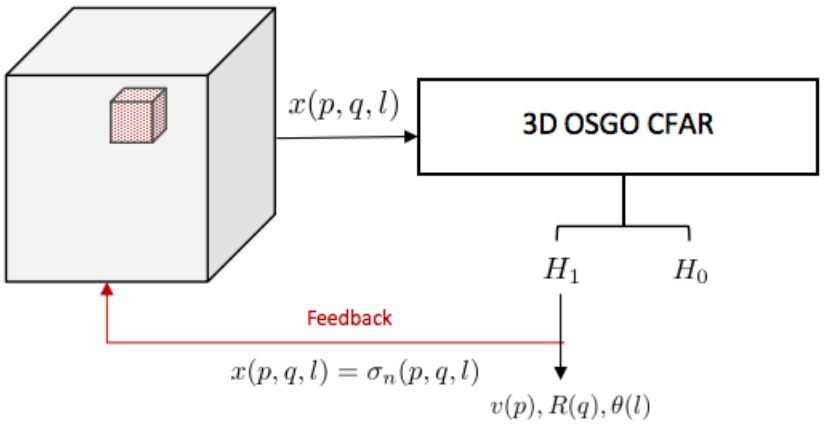

Figure 4.5: 3D OSGO CFAR with improved detection algorithm

The feature array after the feedback of $x(p_0, q_0, l_0)$ can be expressed as

$$\mathbf{X} = x(p,q,l) = \begin{cases} \sigma_n(p_0, q_0, l_0), \ if \ p = p_0, q = q_0, l = l_0 \\ \sum_{j=1}^{L_i} s_{ij}(p,q,l) + n_x(p,q,l), \ other \end{cases} \tag{4.8}$$

4.3 Clustering

After detecting each cell in the feature array $\mathbf{X}$, we can get several measurement vectors $\hat{\mathbf{z}}_u, \ u = 1, \ \ldots, U$. However, as the effects of multipath propagation and noise, one target has multiple corresponding measurement vectors and U is larger than the true number of targets N.

To reduce the effects of multipath propagation and noise, we need a clustering

algorithm without known the number of clusters. In this project, we use density-based spatial clustering of applications with noise (DBSCAN) algorithm to cluster measure vectors and remove the result of miss detection.

Assume that the measure vectors belonging to the same target are in the same cluster. According to the DBSCAN algorithm [4], the measurement vectors which belong to same cluster should satisfy that:

. The normalized distance between the measurement vectors of same cluster (same target) has to be less than the given distance threshold ϵ

. The number of vectors in a cluster must be larger than the given minimum number N_{DBSCAN}

The main idea of DBSCAN algorithm is scanning all vectors and their neighborhoods and checking whether these vectors satisfy the two conditions. If a vector cannot join any cluster, the vector will be defined as noise and be removed.

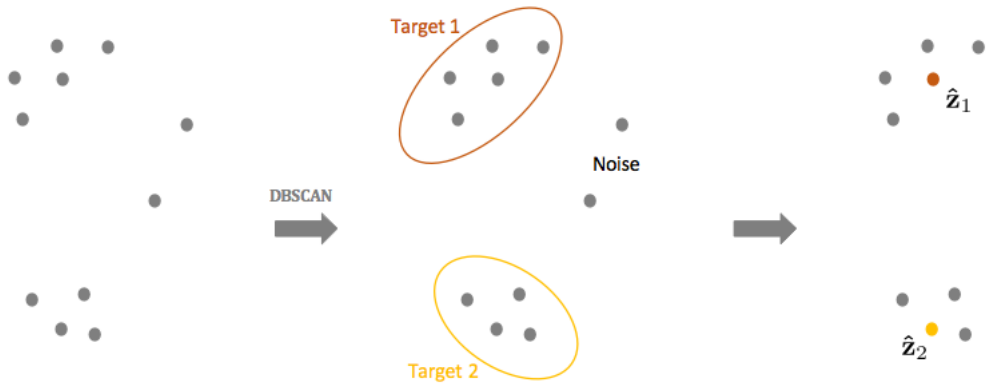

Figure 4.6: Clustering for two targets

After clustering, we select the center vector as the measurement vector of each cluster (each target) to make sure one target correspond to one measurement vector. The measurement vectors after clustering are denoted as $\hat{\mathbf{z}}_g$, $1 \leq g \leq \hat{N}$

$$\hat{\mathbf{z}}_g = [R_g, v_g, \theta_g]^T \tag{4.9}$$

where $\hat{N}$ is the estimate number of targets.

4.4 Conclusion

In this chapter, we have presented an improved multi-target detection algorithm, which is based on OSGO CFAR. We apply the multi-target detection algorithm in the feature matrix and use the clustering algorithm in the detection result to remove the noise and reduce the effect of multipath propagation.

5 Multi-target tracking

The pre-processing part and multi-target detection part are the signal processing for one frame. To detect and track targets in real time, we need to perform the multi-target detection algorithm for each frame. For frame k, the detection results can be rewritten as $\hat{\mathbf{z}}_g(k)$, $0 \leq g \leq \hat{N}(k)$. $\hat{N}(k)$ is the estimate number of targets at k frame. Considering the target appearing and disappearing, $\hat{N}(k)$ can vary with different frame.

5.1 Tracking model

For the multi-target tracking, the detection results $\hat{\mathbf{z}}_g(k) = [R_g(k), v_g(k), \theta_g(k)]^T$, $g = 1, \ , \ldots, \ \hat{N}(k)$ cannot be directly used in the tracking algorithm. The detection results should be matched with the targets of tracking algorithm with data association. The measurement vectors after the data association are denoted as $\mathbf{z}_i(k)$, $i = 1, \ , \ldots, \ \hat{N}(k)$. For the same target, the target index i of $\mathbf{z}_i(k)$ has to be uniform with the previous frames. The multi-target tracking progress is shown in Figure 5.2.

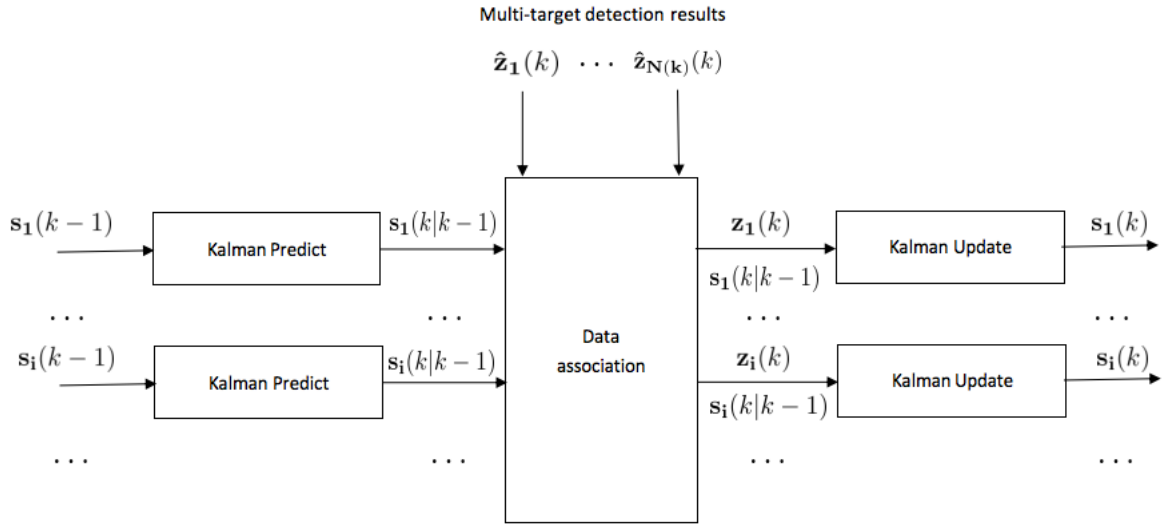

Figure 5.1: Multi-target tracking

Assume that the tracking of different targets is independent. For each target we run separate tracking algorithm. Assume that the multi-target detection and tracking system is a one step Markov system with additive noise. The constant velocity motion

model of target i can be described as

$$\mathbf{s_i}(k) = \mathbf{F}\mathbf{s_i}(k-1) + \mathbf{w_i}(k-1) \tag{5.1}$$

$$\mathbf{z_i}(k) = \mathbf{H}\mathbf{s_i}(k) + \mathbf{v_i}(k) \tag{5.2}$$

where $\mathbf{s_i}(k-1)$ is the state vector of target i at frame $k-1$ with covariance matrix $\mathbf{P_i}(k-1)$. $\mathbf{z_i}(k)$ is the measurement vector of target i at frame k.

Assume the process noise $\mathbf{w_i}(k)$ and the measurement noise $\mathbf{v_i}(k)$ are additive and white Gaussian distributed. The covariance matrix of $\mathbf{w_i}(k)$ is $\mathbf{Q_i}$, while the covariance matrix of $\mathbf{v_i}(k)$ is $\mathbf{R_i}$

$$\mathbf{Q_i} = \begin{bmatrix} 1 & 0 & 0 \\ 0 & 1 & 0 \\ 0 & 0 & 1 \end{bmatrix}$$

$$\mathbf{R_i} = \begin{bmatrix} 2\Delta R & 0 & 0 \\ 0 & 2\Delta v & 0 \\ 0 & 0 & 2\Delta\theta \end{bmatrix} \approx \begin{bmatrix} 1 & 0 & 0 \\ 0 & 1 & 0 \\ 0 & 0 & 12 \end{bmatrix}$$

Assume the target is moving with constant velocity. Then, the state-transition matrix is,

$$\mathbf{F} = \begin{bmatrix} 1 & TN_d & 0 \\ 0 & 1 & 0 \\ 0 & 0 & 1 \end{bmatrix} = \begin{bmatrix} 1 & 0.04 & 0 \\ 0 & 1 & 0 \\ 0 & 0 & 1 \end{bmatrix}$$

where TN_d is the duration time of one frame.

The observation matrix is,

$$\mathbf{H} = \begin{bmatrix} 1 & 0 & 0 \\ 0 & 1 & 0 \\ 0 & 0 & 1 \end{bmatrix}$$

According to the given movement model and the measurement vectors generated by multi-target detection, we can get the state of detected targets for each frame.

5.2 Linear Kalman prediction

As linear Kalman filter is optimal method for the linear model, our multi-target tracking is based on Kalman filter [6].

For target i, the predicted state at frame k is

$$\mathbf{s_i}(k|k-1) = \mathbf{F}\mathbf{s_i}(k-1) \tag{5.3}$$

The predicted covariance at time k is

$$\mathbf{P_i}(k|k-1) = \mathbf{F}\mathbf{P_i}(k-1)\mathbf{F}^T + \mathbf{Q_i} \tag{5.4}$$

We do linear Kalman prediction for each target and obtain the state vectors $\mathbf{s_i}(k|k-1), i = 1, \ , \ldots, \ \hat{N}(k)$.

5.3 Data association

5.3.1 GNN

To associate the detection results with tracking targets, we need to use the Global Nearest Neighbor (GNN) method. By evaluating each observation in track gating region, choose the "best" one to incorporate into track.

We use the Mahalanobis distance [1] between predicted observation $\mathbf{H}\mathbf{s}_i(k|k-1)$ and the multi-target detection result $\hat{\mathbf{z}}_g(k)$ as a matching score of target i and target g. The distance matrix based on Mahalanobis distance can be expressed as

$$\mathbf{D} = d(i,g) = \sqrt{(\hat{\mathbf{z}}_g(k) - \mathbf{H}\mathbf{s_i}(k|k-1))^T \mathbf{P_i}(k|k-1)^{-1} (\hat{\mathbf{z}}_g(k) - \mathbf{H}\mathbf{s_i}(k|k-1))} \tag{5.5}$$

$$1 \leq i \leq \hat{N}(k-1), \ 1 \leq g \leq \hat{N}(k)$$

where $N(k-1)$ is the number of targets at frame $k-1$ and $N(k)$ is the number of targets at frame k. The less Mahalanobis distance $d(i,g)$ is the more possible target i and target g are the same target.

Following the typical GNN method [23], we define a $\hat{N}(k-1) \times \hat{N}(k)$ permutation matrix $\mathbf{A}$, $a(i,g) \in \{0, \ 1\}$, which subject to $a(i,g) = 1$ when target i and target j are matched and $a(i,g) = 0$ when target i and target j are not matched. Each permutation matrix $\mathbf{A}$ denotes one permutation for data association. If $\hat{N}(k-1)$ and $\hat{N}(k)$ are known, there are $\frac{max(\hat{N}(k),\hat{N}(k-1))!}{|\hat{N}(k)-\hat{N}(k-1)|!}$ possible $\mathbf{A}$ permutation matrices.

The score of the permutation matrix $\mathbf{A}$ is defined as

$$e(\mathbf{A}) = \sum_{g=1}^{\hat{N}(k)} \sum_{i=1}^{\hat{N}(k-1)} d(i,g)a(i,g) \tag{5.6}$$

Then, the data association problem will become the problem to find a permutation matrix $\mathbf{A}$ minimizing the score $e(\mathbf{A})$, which can be solved by Hungarian method [16]. Then, we can get the optimal permutation matrix $\mathbf{A}^*$. If $a^*(i,g) = 1$, target i and target g are the same target. The measurement vector of target i at frame k is

$$\mathbf{z_i}(k) = \hat{\mathbf{z}}_g(k), \ a^*(i,g) = 1 \tag{5.7}$$

$$a^*(i,g) = 1, 1 \leq i \leq \hat{N}(k)$$

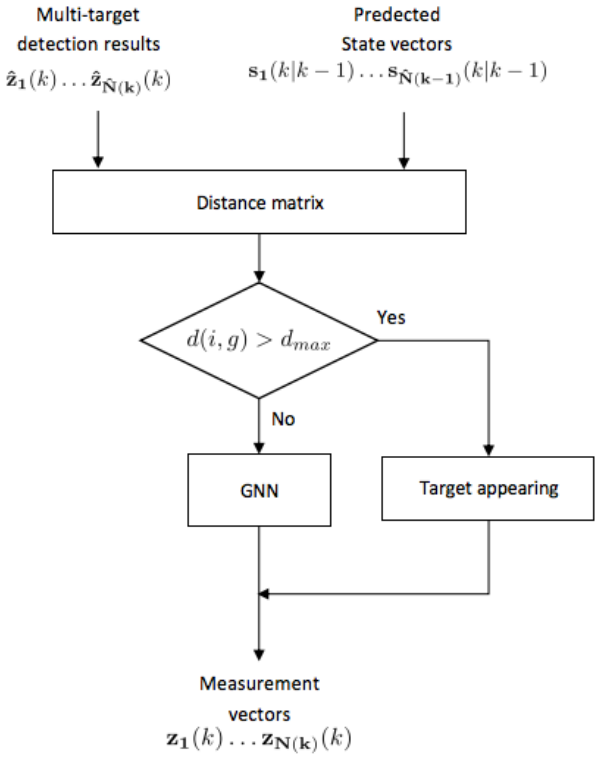

Figure 5.2: Data association

Consider the targets appearing, we add distance checking to the basic GNN algorithm. Assume that if target i and target g are the same target, the maximum distance is d_{max}. If $\forall i : d(i,g) > d_{max}$, we define that target g is a new appearing target, which will be given a new target index following i.

5.4 Linear Kalman update

We use the measurement vectors after data association to update the state vectors of corresponding target.
For target i, the Kalman gain is

$$\mathbf{K_i} = \mathbf{P_i}(k|k-1)\mathbf{H}^T(\mathbf{H}\mathbf{P_i}(k|k-1)\mathbf{H}^T + \mathbf{R_i})^{-1} \tag{5.8}$$

The updated state of target i at frame k is

$$\mathbf{s_i}(k) = \mathbf{s_i}(k|k-1) + \mathbf{K_i}(\mathbf{z_i}(k) - \mathbf{H}\mathbf{s_i}(k|k-1)) \tag{5.9}$$

$$\mathbf{s_i}(k) = [\hat{R}_i, \hat{v}_i, \hat{\theta}_i]^T \tag{5.10}$$

$\mathbf{s_i}(k)$ contains the smoothed estimate of range, Doppler velocity, and angle, which are the output of the signal processing of FMCW radar system.

The updated covariance matrix of target i at frame k is

$$\mathbf{P_i}(k) = (1 - \mathbf{K_i H})\mathbf{P_i}(k|k-1) \tag{5.11}$$

which will be used into the tracking for the next frame.

5.5 Conclusion

In this chapter, we derive a low-complexity multi-target tracking algorithm to track targets. The tracking algorithm uses the data association to associate target states at different frames, then track each target independently. After multi-target tracking, we can obtain range, Doppler velocity, and angle of targets, which are also the final results of signal processing.

6 Simulation and Evaluation

The simulation of target motion is based on the Headed social force model (HSFM) [5]. Assume that the maximum range of radar is 10 m, and the field of view is a 120 deg sector with 10 m radius. Assume that the minimum distance between two targets and the minimum distance between target and boundary of field of view are both 0.5 m.

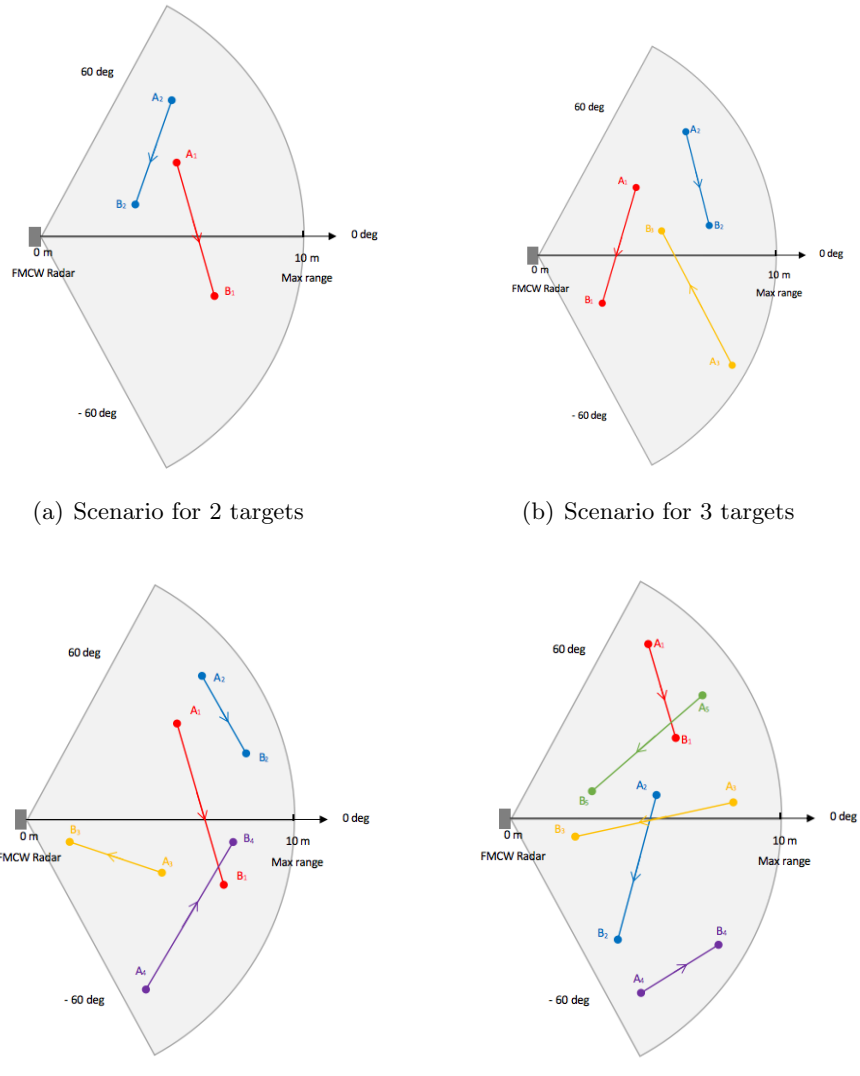

(a) Scenario for 2 targets

(b) Scenario for 3 targets

(c) Scenario for 4 targets

(d) Scenario for 5 targets

Figure 6.1: The sketches of target trails for different scenarios

We have scenarios for two, three, four, and five targets. Each scenario repeats 500 random linear motion trails. The sketches of target trails for four scenarios are shown in Figure 6.1.

In this project, we use the Root Mean Square Error (RMSE) to evaluate the tracking results. The RMSE of range, angle and Doppler velocity are shown as follow:

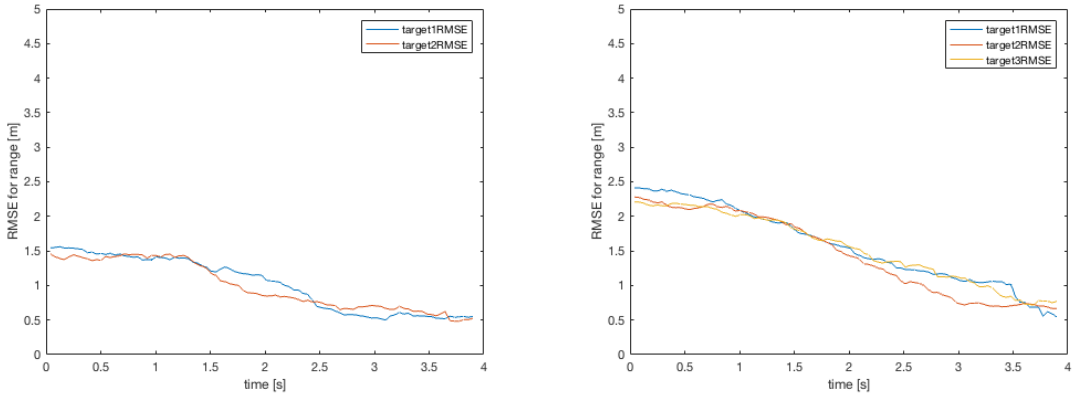

(a) RMSE for 2 targets

(b) RMSE for 3 targets

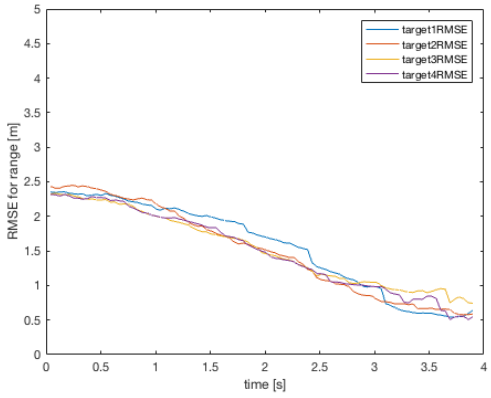

(c) RMSE for 4 targets

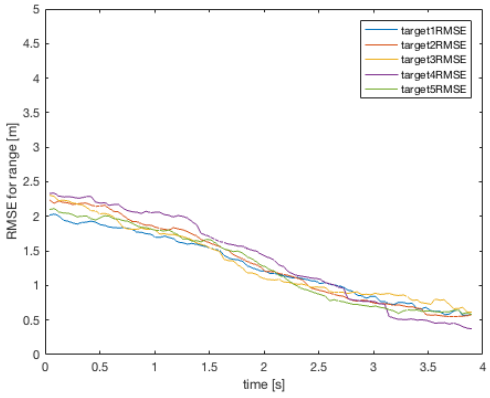

(d) RMSE for 5 targets

Figure 6.2: Range RMSE

From Figure 6.2, the RMSE of range for different targets can decrease to 0.5m after tracking. Comparing with the results of two targets, the RMSEs of range for other scenarios are higher at the beginning but can be decreased effectively after tracking.

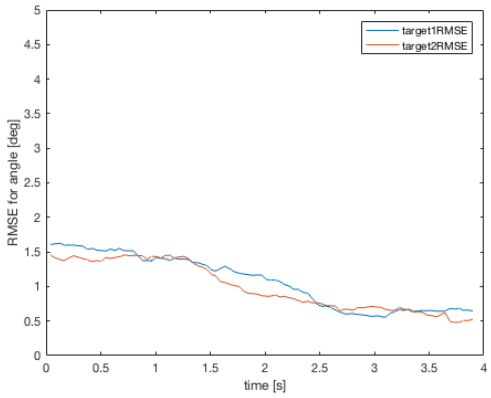

(a) RMSE for 2 targets

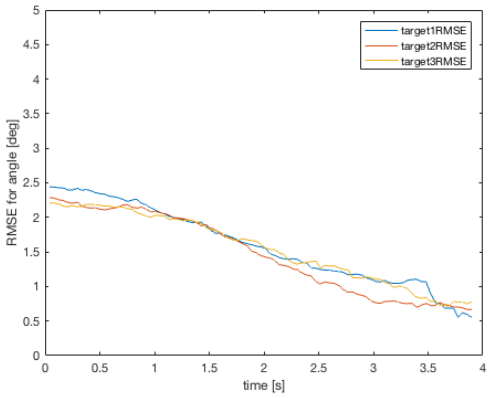

(b) RMSE for 3 targets

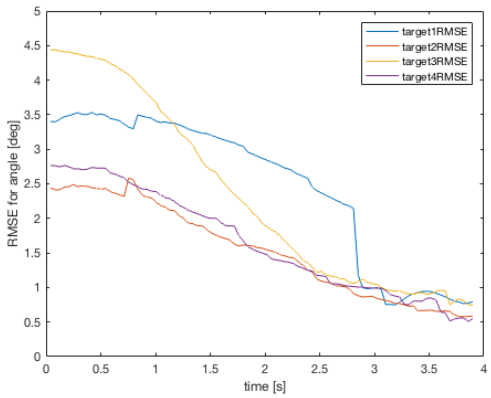

(c) RMSE for 4 targets

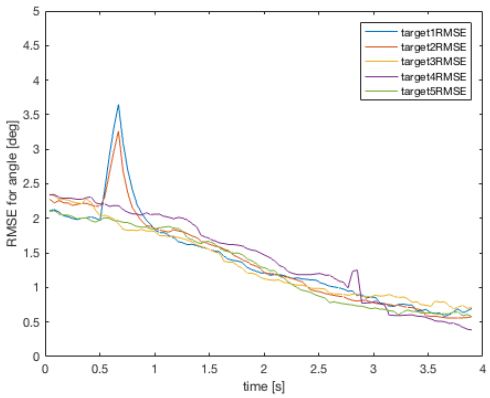

(d) RMSE for 5 targets

Figure 6.3: Angle RMSE

Similar to the RMSE of range, the RMSE of angle for different targets can also decrease to 0.5 deg after tracking. However, as the angle resolution $\Delta\theta$ is larger than the range resolution, to accurately detect the angle of targets is more difficult than range. From Figure 6.3, when increasing the number of targets, there are some fluctuations during the tracking.

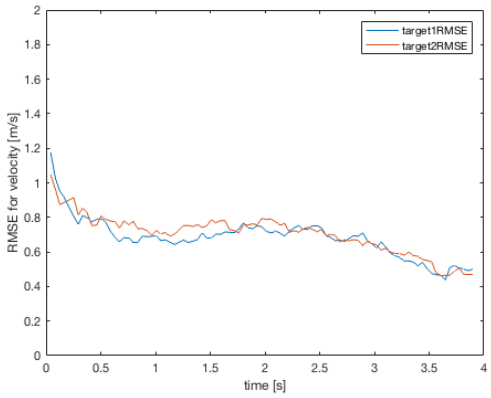

(a) RMSE for 2 targets

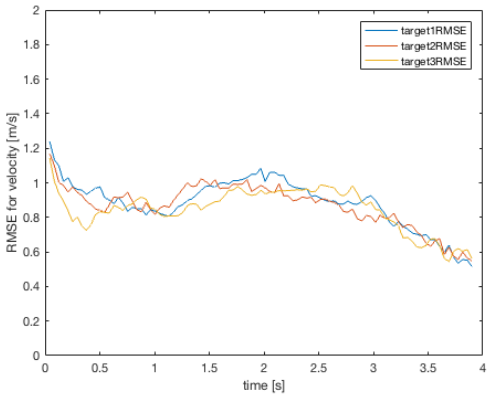

(b) RMSE for 3 targets

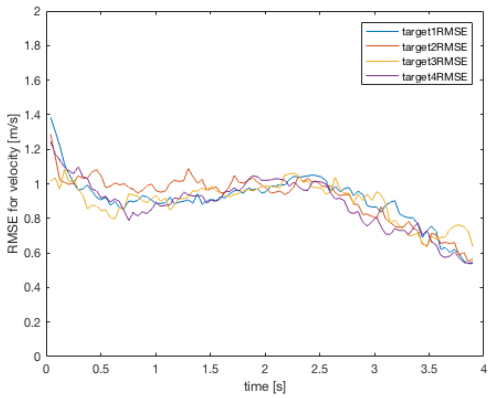

(c) RMSE for 4 targets

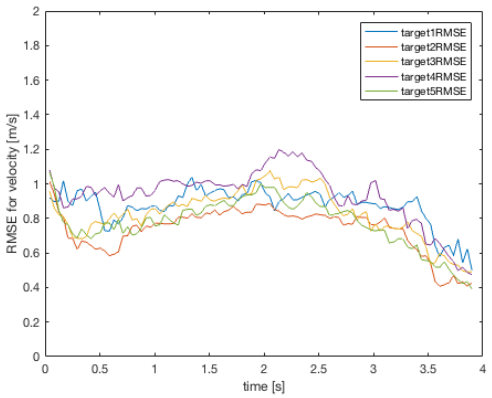

(d) RMSE for 5 targets

Figure 6.4: Doppler velocity RMSE

From Figure 6.4, the RMSE of Doppler velocity decrease rapidly in the beginning and end but tend to flatten out in the middle. Because the simulation assumes that the target walking from the start point needs to accelerate from rest, while the target close to the end point needs to accelerate slow down to rest.

6.1 Conclusion

In this chapter, we simulated the motion trails and designed four scenarios with different number of targets. For each scenario, we use the RMSE to evaluate the results of 500 Monte Carlo simulations. Comparing the results of different scenarios, we can see that multi-target detection and tracking algorithm has a good performance for the cases with two and three targets. But when the number of targets increases, the accuracy of angle results will decrease.

7 Experimental Validation

7.1 Experimental platform

In this project, the experimental platform is an 8 GHz FMCW radar system, which can be seen in Figure 7.1. The transmitting antenna and receiving antenna are both frequency scanning antenna with "rampart" shape. The FMCW radar system receives the echo signal from targets. After mixing, ADC sampling, and low-pass filtering, the radar system will output the beat frequent signal. The subsequent signal processing steps (pre-processing, multi-target detection, and tracking) will be completed in MATLAB.

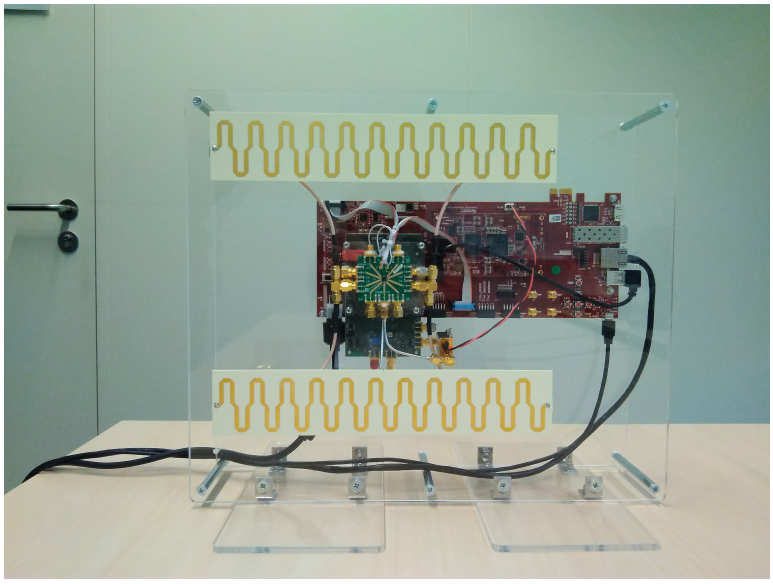

Figure 7.1: FMCW radar platform

The parameters of radar system are shown on Table 7.1. The parameters of radar system for simulation and experiment are the same. The results of simulation and experiment will be compared in the next section.

Parameters	Value
Bandwidth(B)	1 GHz
Starting frequency(f_c)	7.3 GHz
Interval between two chirps(T)	2.6 ms
Sweep time(T_c)	0.082 ms
Number of chirps per frame(N_d)	16
Number of samples per chirp(M)	512
Interval between two frames	0.0416 s

Table 7.1: Parameters of the 8 GHz FMCW radar system

7.2 Experimental Results

The experimental environment is a room with 7.08 m width and 11.75 m length. The field of view of the experimental FMCW radar system is shown as the light gray area in Figure 7.2. We establish a polar coordinate system and set the position of FMCW radar as the origin point. The scanning angle is from -60 deg to 60 deg.

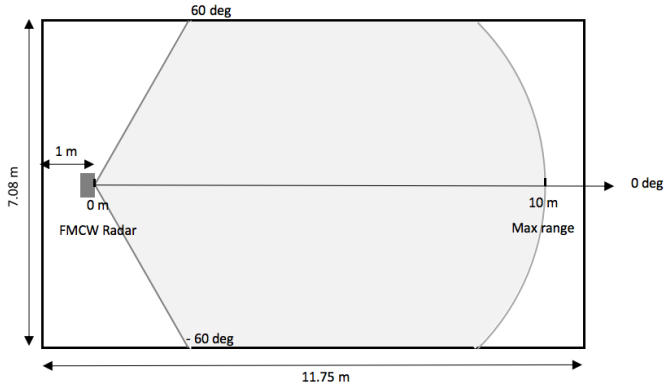

Figure 7.2: Experiment environment

To valuate the performance of two targets detection and tracking, we design four scenarios.

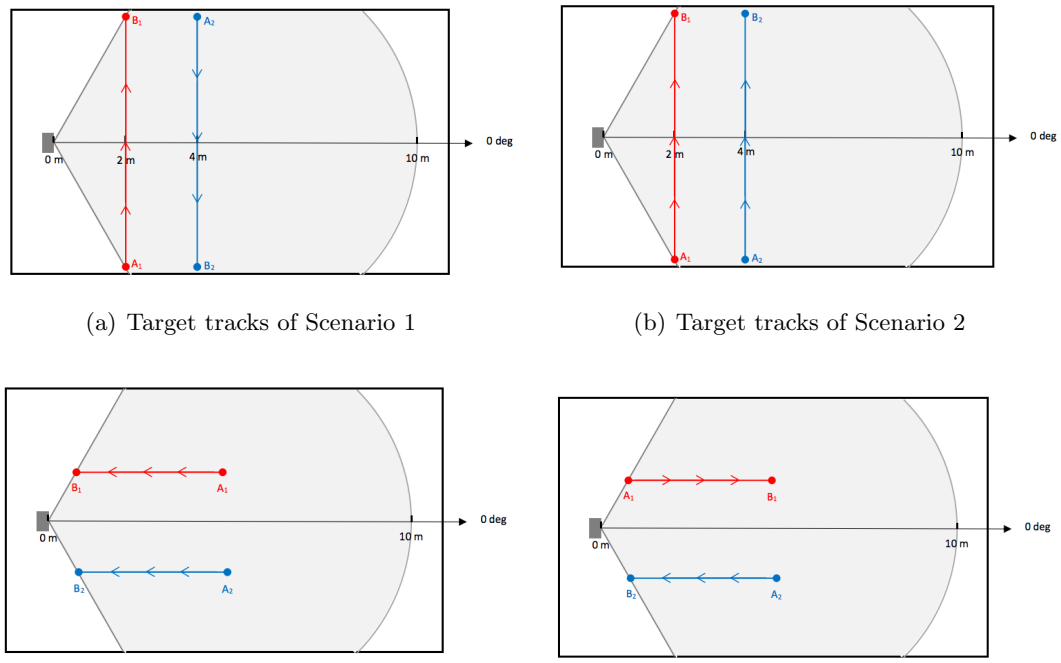

(a) Target tracks of Scenario 1

(b) Target tracks of Scenario 2

(c) Target tracks of Scenario 3

(d) Target tracks of Scenario 4

Figure 7.3: Target tracks for different scenarios

. **Scenario 1**:
Target 1 was walking back and forth between the two points $A_1(4, -\pi/3)$ and $B_1(4, \pi/3)$, while target 2 was walking back and forth between the two points $A_2(5.34, 0.7245)$ and $B_2(5.34, -0.7245)$. A_1 and A_2 were the start points of target 1 and target 2. The track of target 1 and target 2 were parallel but moving with opposite directions (Figure 7.3(a)).

This scenario mainly considered the case of target crossing. The tracking result of scenario 1 is shown in Figure 7.4. Although the range result of target 1 was miss detected when target crossed, tracking algorithm can still keep accurate track after target crossing.

. **Scenario 2**:
Similar to Scenario 1, the tracks of target 1 and target 2 for Scenario 2 were also parallel. However, the direction of two targets were same (Figure 7.3(b)). A_1 and B_1 were not changed, but A_2 and B_2 would exchange, i.e. $A_2(5.34, -0.7245)$ and $B_2(5.34, 0.7245)$.

This scenario showed the effect of the target masking. The signal of the masked target was much weaker than the other one, which would increase the difficulties of detection and tracking. The tracking result of scenario 2 is shown in Figure 7.5. The results of target 1 (masked target) had more miss detection

than the other target.

. **Scenario 3**:
Target 1 was walking back and forth between the two points $A_1(5, \pi/12)$ and $B_1(1.5, \pi/3)$, while target 2 was walking back and forth between the two points $A_2(5, -\pi/12)$ and $B_2(1.5, -\pi/3)$. The tracks of target 1 and target 2 were parallel but moving with the same direction (Figure 7.3(c)).

This scenario mainly considered the case of targets with the same Doppler velocity and the same range, which had a high requirement for data association. The tracking results of scenario 3 were shown in Figure 7.6. As there was no target masking, comparing with other scenarios, this scenario had the best performance. The experimental results were matched with simulation results.

. **Scenario 4**:
Similar to Scenario 3, the tracks of target 1 and target 2 for Scenario 4 were also parallel, but the direction of the two targets are opposite (Figure 7.3(d)).

The tracking result of scenario 4 is shown in Figure 7.7. The experimental results of range and Doppler velocity were matched with simulation results. However, the results of the angle were a bit worse.

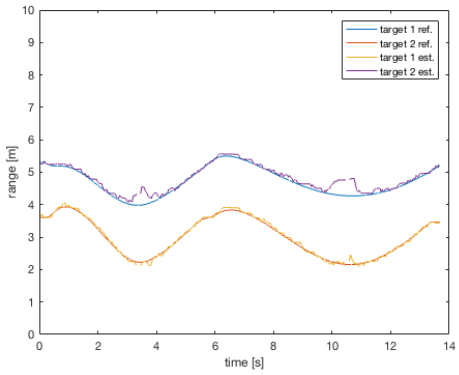

(a) Simulation result of range

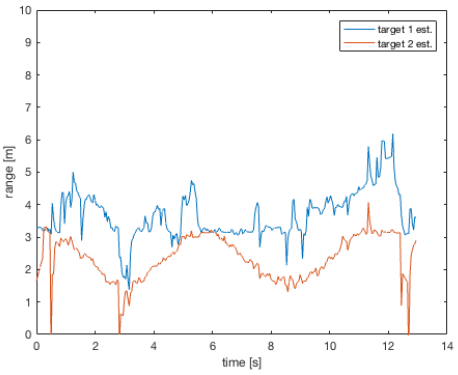

(b) Experimental result of range

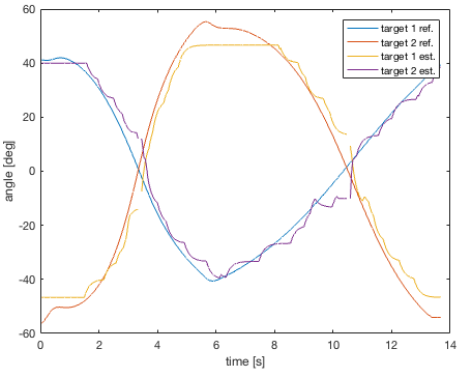

(c) Simulation result of angle

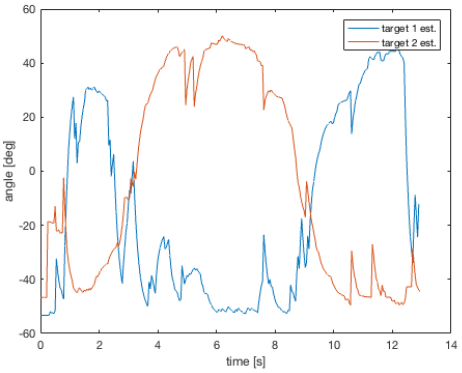

(d) Experimental result of angle

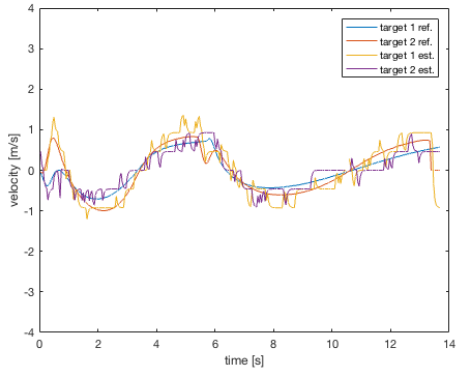

(e) Simulation result of Doppler velocity

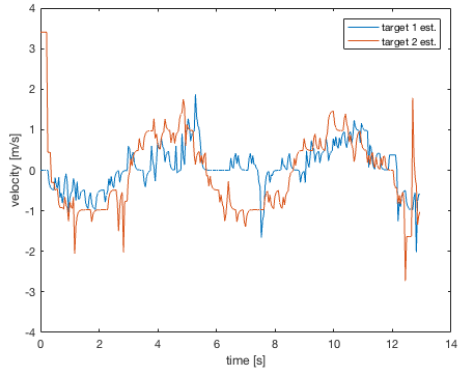

(f) Experimental result of Doppler velocity

Figure 7.4: The results of Scenario 1

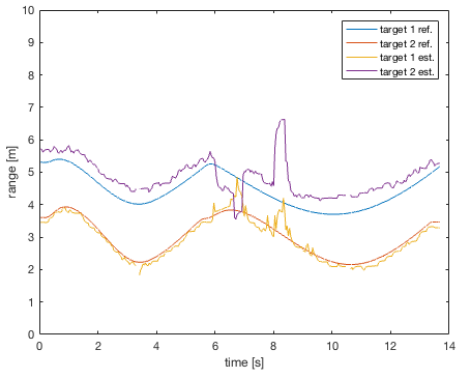

(a) Simulation result of range

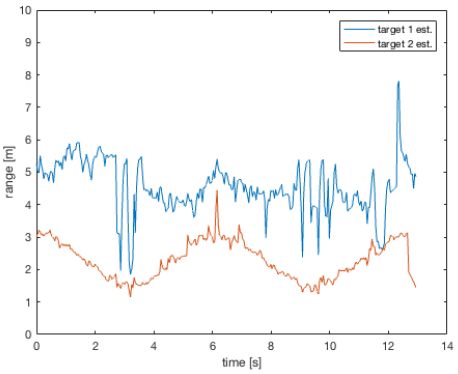

(b) Experimental result of range

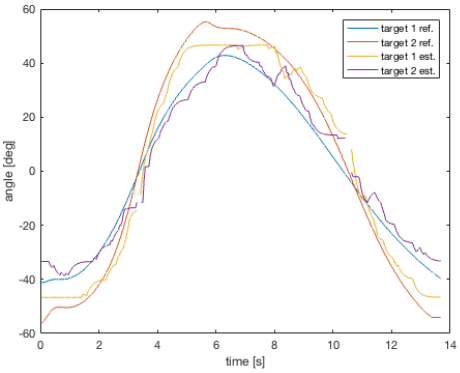

(c) Simulation result of angle

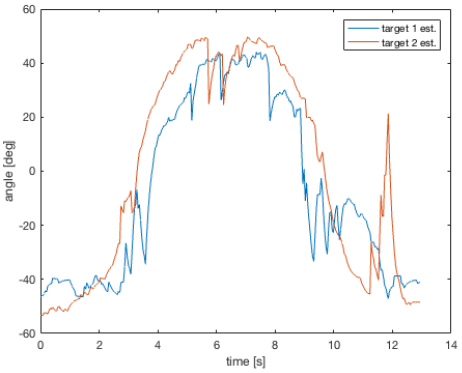

(d) Experimental result of angle

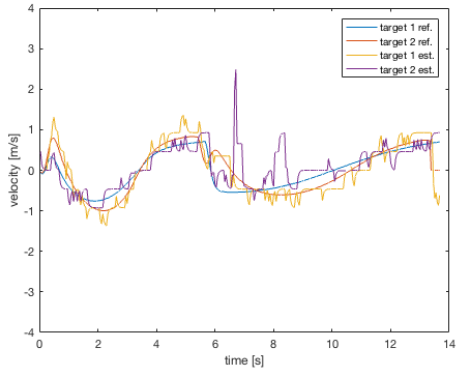

(e) Simulation result of Doppler velocity

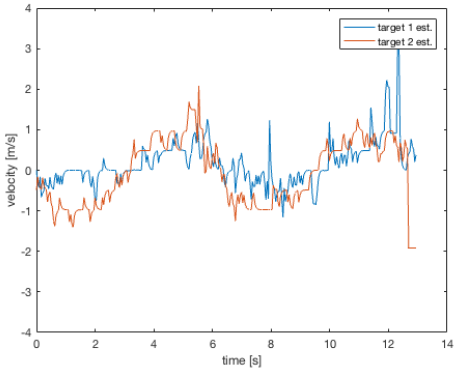

(f) Experimental result of Doppler velocity

Figure 7.5: The results of Scenario 2

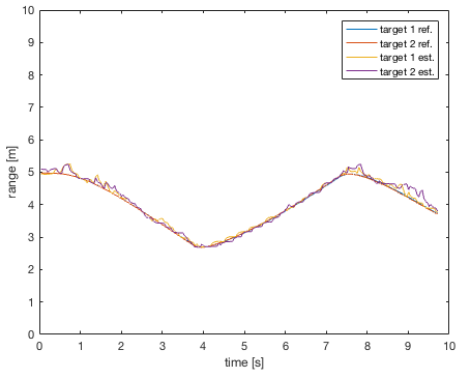

(a) Simulation result of range

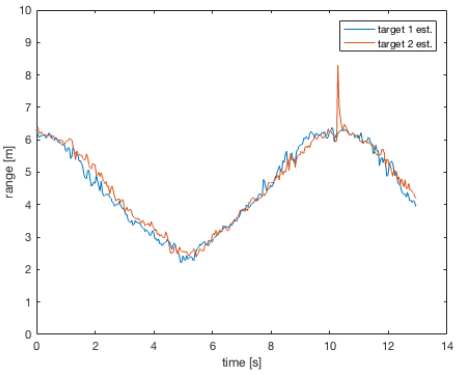

(b) Experimental result of range

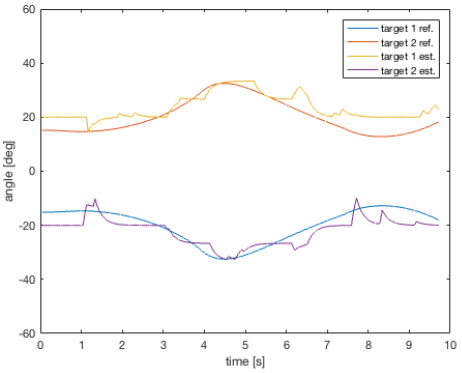

(c) Simulation result of angle

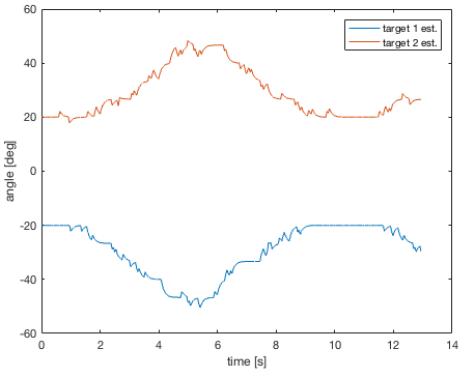

(d) Experimental result of angle

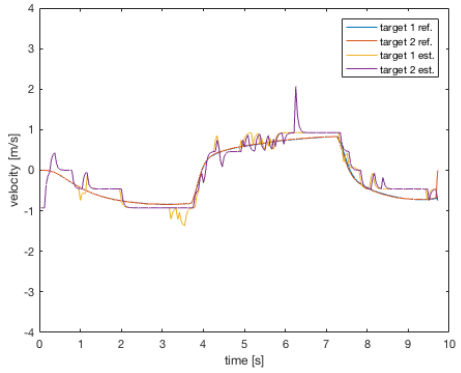

(e) Simulation result of Doppler velocity

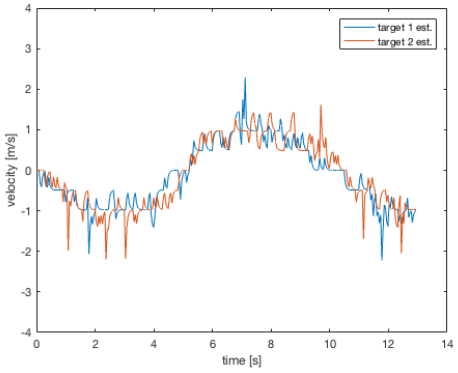

(f) Experimental result of Doppler velocity

Figure 7.6: The results of Scenario 3

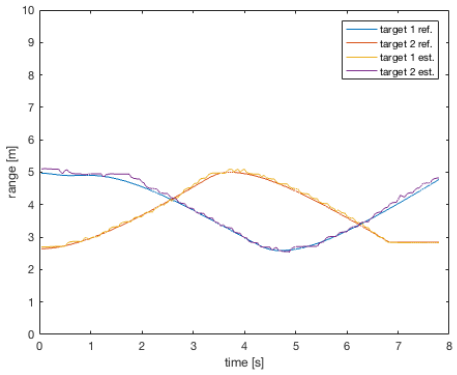

(a) Simulation result of range

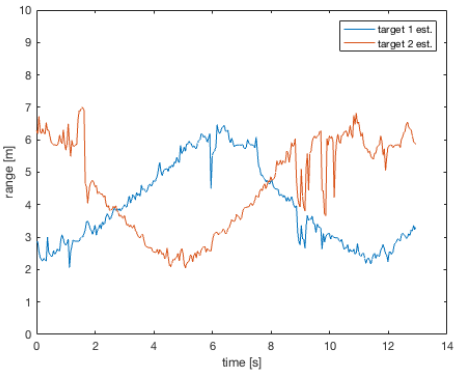

(b) Experimental result of range

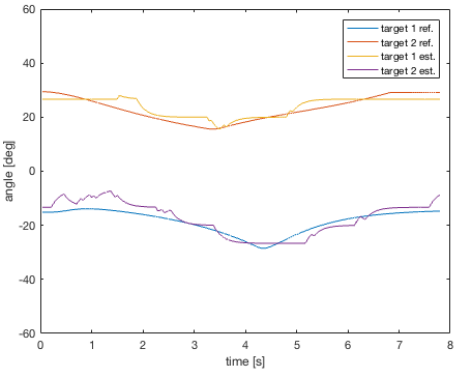

(c) Simulation result of angle

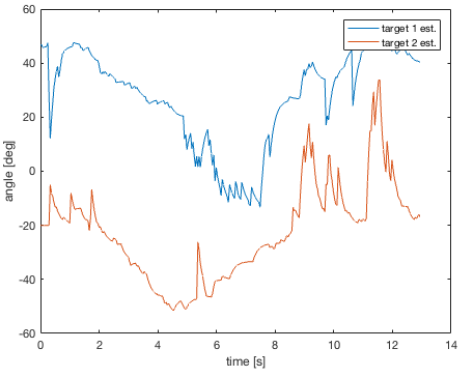

(d) Experimental result of angle

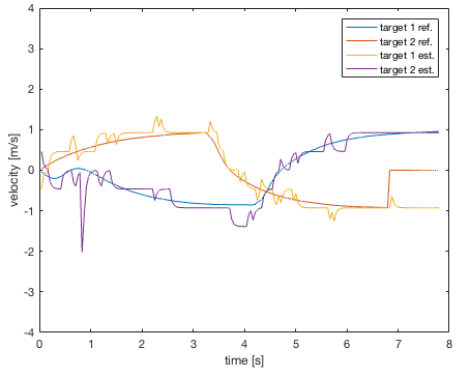

(e) Simulation result of Doppler velocity

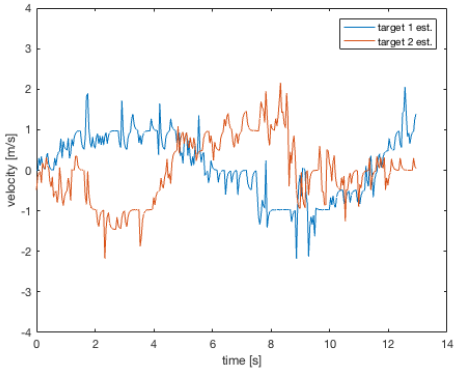

(f) Experimental result of Doppler velocity

Figure 7.7: The results of Scenario 4

7.3 Conclusion

In this chapter, we designed four typical scenarios for simulation and experiment. We compared and analyzed the simulation results and experimental results for different

scenarios. In summary, most of the experimental results were matched with simulation results. Comparing with simulation and experimental results, we can clearly see that target masking has produced the influence that can't be ignored in the real environment.

8 Conclusion and future work

8.1 Conclusion

The aim of this thesis project is to explore the multi-target detection and tracking algorithms with an 8 GHz SISO FMCW. According to the new signal processing based on the SISO system, the angle information of targets can be obtained by a time-domain sliding window, while the range and Doppler velocity information can be obtained by 2D FFT. We use the multi-target detection algorithm based on OSGO CFAR to detect targets from 3D feature array and obtain the range, Doppler velocity, and angle information of targets. For the multi-target tracking algorithm, independent tracking and data association are used to track and estimate the position and velocity of targets.

According to the results of simulation and experiment, the multi-target detection and tracking have a good performance for different scenarios. The detection and tracking algorithm can clearly distinguish different targets.

8.2 Future work

However, the current algorithm still has some shortages. For the results of simulation and experiment, the accuracy of Doppler velocity is lower than range and angle. Besides, the current tracking is based on the single linear motion model, but the motion in the real environment is usually nonlinear.

To improve the multi-target detection and tracking algorithm, some recommendations are presented to extend this research:

. The current algorithm uses 16 chirps per frame in Doppler FFT. To increase the accuracy of Doppler velocity, we can double the number of chirps per frame (N_d) and half the interval time between chirps(T), which can keep the interval time between two frames. This improvement needs some hardware improvements of the FMCW radar system.

. To improve the tracking algorithm, nonlinear method[21] and Interaction Multiple Model (IMM) [2, 22] can be used in the future. Comparing with the tracking algorithm based on the linear Kalman filter, the nonlinear and multiply model methods can better model the motion of the real target.

Bibliography

[1] Roy De Maesschalck, Delphine Jouan-Rimbaud, and Désiré L Massart. The mahalanobis distance. *Chemometrics and intelligent laboratory systems*, 50(1):1–18, 2000.

[2] Hans Driessen and Yvo Boers. An efficient particle filter for jump Markov nonlinear systems. 2004.

[3] Antoni Elias Fusté, García G de Mercado, Elías de los Reyes, et al. Analysis of some modified ordered statistic CFAR: OSGO and OSSO CFAR. *IEEE Transactions on Aerospace and Electronic Systems*, 26(1):197–202, 1990.

[4] Martin Ester, Hans-Peter Kriegel, Jörg Sander, Xiaowei Xu, et al. A density-based algorithm for discovering clusters in large spatial databases with noise. In *Kdd*, volume 96, pages 226–231, 1996.

[5] Francesco Farina, Daniele Fontanelli, Andrea Garulli, Antonio Giannitrapani, and Domenico Prattichizzo. Walking ahead: The headed social force model. *PloS one*, 12(1), 2017.

[6] Rudolf Frühwirth. Application of Kalman filtering to track and vertex fitting. *Nuclear Instruments and Methods in Physics Research Section A: Accelerators, Spectrometers, Detectors and Associated Equipment*, 262(2-3):444–450, 1987.

[7] Prashant P Gandhi and Saleem A Kassam. Analysis of CFAR processors in nonhomogeneous background. *IEEE Transactions on Aerospace and Electronic systems*, 24(4):427–445, 1988.

[8] Hana Godrich, Vlad M Chiriac, Alexander M Haimovich, and Rick S Blum. Target tracking in MIMO radar systems: Techniques and performance analysis. In *2010 IEEE Radar Conference*, pages 1111–1116. IEEE, 2010.

[9] Shaohua Hong, Lin Wang, Zhi-Guo Shi, and Kang Sheng Chen. Simplified particle PHD filter for multiple-target tracking: Algorithm and architecture. *Progress In Electromagnetics Research*, 120:481–498, 2011.

[10] Chung-Jung Huang, Chia-Wei Dai, Tsung-Yu Tsai, Wei-Ho Chung, and Ta-Sung Lee. A closed-form phase-comparison ML DOA estimator for automotive radar with one single snapshot, 01 2013.

[11] Eugin Hyun, Young-Seok Jin, and Jong-Hun Lee. A pedestrian detection scheme using a coherent phase difference method based on 2D range-doppler FMCW radar. *Sensors*, 16(1):124, 2016.

[12] Eugin Hyun, Young-Seok Jin, and Jong-Hun Lee. Moving and stationary target detection scheme using coherent integration and subtraction for automotive FMCW radar systems. In *2017 IEEE Radar Conference (RadarConf)*, pages 0476–0481. IEEE, 2017.

[13] Snezhana Jovanoska and Reiner Thomä. Multiple target tracking by a distributed UWB sensor network based on the PHD filter. In *2012 15th International Conference on Information Fusion*, pages 1095–1102. IEEE, 2012.

[14] Dae-Bong Kim and Sun-Mog Hong. Multiple-target tracking and track management for an FMCW radar network. *EURASIP Journal on Advances in Signal Processing*, 2013(1):159, 2013.

[15] Matthias Kronauge and Hermann Rohling. Fast two-dimensional CFAR procedure. *IEEE Transactions on Aerospace and Electronic Systems*, 49(3):1817–1823, 2013.

[16] Harold W Kuhn. The Hungarian method for the assignment problem. *Naval research logistics quarterly*, 2(1-2):83–97, 1955.

[17] Krzysztof Kulpa. The CLEAN type algorithms for radar signal processing. In *2008 Microwaves, Radar and Remote Sensing Symposium*, pages 152–157. IEEE, 2008.

[18] Moon-Sik Lee and Yong-Hoon Kim. Design and performance of a 24-ghz switch-antenna array FMCW radar system for automotive applications. *IEEE Transactions on Vehicular Technology*, 59(5):2290–2297, 2010.

[19] Yi-An Li, Meng-Hsiung Hung, Shih-Jou Huang, and Jri Lee. A fully integrated 77GHz FMCW radar system in 65nm CMOS. In *2010 IEEE International Solid-State Circuits Conference-(ISSCC)*, pages 216–217. IEEE, 2010.

[20] Jau-Jr Lin, Yuan-Ping Li, Wei-Chiang Hsu, and Ta-Sung Lee. Design of an FMCW radar baseband signal processing system for automotive application. *SpringerPlus*, 5(1):42, 2016.

[21] Raja Manish. Linear and non-linear estimation techniques: Theory and comparison. *arXiv preprint arXiv:1406.5556*, 2014.

[22] Efim Mazor, Amir Averbuch, Yakov Bar-Shalom, and Joshua Dayan. Interacting multiple model methods in target tracking: a survey. *IEEE Transactions on aerospace and electronic systems*, 34(1):103–123, 1998.

[23] J. McMillan and Sang Seok Lim. Data association algorithms for multiple target tracking. page 37, 07 1990.

[24] Pavlo Molchanov, Shalini Gupta, Kihwan Kim, and Kari Pulli. Short-range FMCW monopulse radar for hand-gesture sensing. In *2015 IEEE Radar Conference (RadarCon)*, pages 1491–1496. IEEE, 2015.

[25] Sujeet Milind Patole, Murat Torlak, Dan Wang, and Murtaza Ali. Automotive radars: A review of signal processing techniques. *IEEE Signal Processing Magazine*, 34(2):22–35, 2017.

[26] Zhengyu Peng, José-María Muñoz-Ferreras, Roberto Gómez-García, and Changzhi Li. FMCW radar fall detection based on ISAR processing utilizing the properties of rcs, range, and doppler. In *2016 IEEE Mtt-S International Microwave Symposium (IMS)*, pages 1–3. IEEE, 2016.

[27] Prajoy Podder, Tanvir Zaman Khan, Mamdudul Haque Khan, and M Muktadir Rahman. Comparative performance analysis of hamming, hanning and blackman window. *International Journal of Computer Applications*, 96(18), 2014.

[28] Hermann Rohling. Radar CFAR thresholding in clutter and multiple target situations. *IEEE transactions on aerospace and electronic systems*, (4):608–621, 1983.

[29] Adel AM Saleh and Reinaldo Valenzuela. A statistical model for indoor multipath propagation. *IEEE Journal on selected areas in communications*, 5(2):128–137, 1987.

[30] Roman Streubel and Bin Yang. Fusion of stereo camera and MIMO-FMCW radar for pedestrian tracking in indoor environments. In *2016 19th International Conference on Information Fusion (Fusion)*, pages 565–572. IEEE, 2016.

[31] Li Su, Hsien Shun Wu, and Ching-Kuang C Tzuang. 2-D FFT and time-frequency analysis techniques for multi-target recognition of FMCW radar signal. In *Asia-Pacific Microwave Conference 2011*, pages 1390–1393. IEEE, 2011.

[32] Luis Úbeda-Medina and Jesús Grajal. Multiple target tracking in the fully adaptive radar framework. In *2016 IEEE Statistical Signal Processing Workshop (SSP)*, pages 1–5. IEEE, 2016.

[33] Baptist Vandersmissen, Nicolas Knudde, Azarakhsh Jalalvand, Ivo Couckuyt, André Bourdoux, Wesley De Neve, and Tom Dhaene. Indoor person identification using a low-power FMCW radar. *IEEE Transactions on Geoscience and Remote Sensing*, 56(7):3941–3952, 2018.

[34] Damien Vivet, Paul Checchin, and Roland Chapuis. Localization and mapping using only a rotating FMCW radar sensor. *Sensors*, 13(4):4527–4552, 2013.

[35] Guochao Wang, Changzhan Gu, Takao Inoue, and Changzhi Li. Hybrid FMCW-interferometry radar system in the 5.8 GHz ISM band for indoor precise position and motion detection. In *2013 IEEE MTT-S International Microwave Symposium Digest (MTT)*, pages 1–4. IEEE, 2013.

[36] Volker Winkler. Range Doppler detection for automotive FMCW radars. In *2007 European Radar Conference*, pages 166–169. IEEE, 2007.

[37] Andrzej Wojtkiewicz, Jacek Misiurewicz, M Nalecz, Konrad Jedrzejewski, and Krzysztof Kulpa. Two-dimensional signal processing in FMCW radars. *Proc. XX KKTOiUE*, pages 475–480, 1997.

[38] Chunmei Xu, Yang Li, Chao Ji, Yongming Huang, Haiming Wang, and Yili Xia. An improved CFAR algorithm for target detection. In *2017 International Symposium on Intelligent Signal Processing and Communication Systems (ISPACS)*, pages 883–888. IEEE, 2017.

[39] Lijia Zhu, Yuanqing Chen, Wei Shi, Hongwei Wang, and Guangli Yang. A K-band low-cost phase shifter for short-range FMCW radar applications. In *2018*

International Applied Computational Electromagnetics Society Symposium-China (ACES), pages 1–2. IEEE, 2018.